LOW-COST SMARTPHONE-OPERATED READOUT SYSTEM FOR POINT-OF-CARE ELECTROCHEMICAL AND PHOTOELECTROCHEMICAL BIOSENSING

LOW-COST SMARTPHONE-OPERATED READOUT SYSTEM FOR POINT-OF-CARE ELECTROCHEMICAL AND PHOTOELECTROCHEMICAL BIOSENSING

By ALEXANDER SCOTT, B.Eng., B.Sc.

A Thesis Submitted to the School of Graduate Studies in Partial Fulfilment of the Requirements for the Degree Master of Applied Sciences

McMaster University MASTER OF APPLIED SCIENCE (2021) Hamilton, Ontario (Biomedical Engineering)

TITLE	Low-Cost Smartphone-Operated Readout System for Point-of-Care Electrochemical and Photoelectrochemical Biosensing
AUTHOR	Alexander Scott
	B.Eng. and B.Sc. (University of Saskatchewan)
SUPERVISOR	Dr. L. Soleymani
NUMBER OF PAGES	xii, 86

Lay Abstract

Early and prompt detection of disease biomarkers is crucial in order to develop effective disease management strategies. Unfortunately, many gold-standard diagnostic techniques for infectious diseases, cancers, heart diseases, among other conditions prove to be time-consuming, costly, and reliant on trained professionals in a laboratory setting. Electrochemical and photoelectrochemical detection are two sensing modalities that show promising potential for point-of-care applications, as they are easily miniaturized, inexpensive, and can be used to detect both the presence of and the amount of analyte present. However, up until now, these sensing modalities have mostly been confined to research settings. To expedite the commercialization of such sensors and to facilitate their translation to point-of-care diagnostics, we have developed a low-cost smartphone-operated electrochemical and photoelectrochemical readout system. Through the integration of peripheral instruments including a sample heater, electromagnet, and optical excitation source, this system is compatible with a number of different biosensors.

Abstract

Despite the increasing number of electrochemical and photoelectrochemical biosensors reported in the research literature, few have achieved success outside of a laboratory setting. This can partly be attributed to accessibility issues with commercially available readout instruments. Consequently, low-cost and portable readout instruments have been developed by researchers, but these devices fail to address other key compatibility and accessibility challenges. Much like the commercial systems, these devices are not natively compatible with multiplexed signal assays consisting of two or more working electrodes, cannot control optical excitation sources for photoelectrochemical biosensing, nor can they interface with auxiliary instruments such as heaters and electromagnets. To this end, we have developed a low-cost smartphone-operated electrochemical and photoelectrochemical readout system for point-of-care biosensing. Our readout system can perform standard voltammetric techniques and is capable of synchronously controlling an optical excitation source to support photoelectrochemical biosensing. This device is compatible with standard three-electrode assays as well as dual signal assays with two working electrodes. We have also created a portable sample heater that can be controlled by this readout system to facilitate on-site sample heating and have also integrated a portable electromagnet to perform away-from-lab magnetic manipulation.

Table of Contents

List of Figures

List of Tables

List of abbreviations

AA	Ascorbic acid
ADC	Analog-to-digital converter
BLE	Bluetooth low energy
CAmp	Control Amplifier
CA	Caffeic acid
CE	Counter electrode
COVID-19	Coronavirus disease of 2019
CV	Cyclic voltammetry
DAC	Digital-to-analog converter
DMSO	Dimethyl sulfoxide
DNA	Deoxyribonucleic acid
DP	Differential Pulse
E. coli	Escherichia coli
EDC	1-ethyl-3-(3-dimethylaminopropyl)carbodiimide hydrochloride
EDTA	Ethylenediaminetetraacetic acid
EIS	Electrochemical impedance spectroscopy
ELISA	Enzyme-linked immunosorbent assay
FNA	Functional nucleic acid
ITO/PET	Indium tin oxide/poly(ethylene terephthalate)
LED	Light emitting diode
LS	Linear sweep
MCH	Mercapto hexanol
MES	2-(N-morpholino)ethanesulfonic acid
NC	Non-complimentary

NHS	N-hydroxysulfosuccinimide
NP	Normal pulse
PBS	Phosphate buffer solution
PCB	Printed circuit board
PCR	Polymerase chain reaction
PEC	Photoelectrochemistry/photoelectrochemical
PoC	Point-of-care
QR	Quick response
RE	Reference electrode
RNA	Ribonucleic acid
RT	Room temperature
SCE	Saturated calomel electrode
SHE	Standard hydrogen electrode
SPS	Samples per second
ssDNA	Single-stranded DNA
SWV	Square wave voltammetry
TBE	Tris-borate-EDTA buffer
TD	thiolated DNAzyme
TIA	Transimpedance amplifier
TP	Thiolated probe
USB	Universal serial bus
UV	Ultraviolet
VF	Voltage follower
WE	Working electrode

Acknowledgement

The completion of this thesis would not have been possible if it weren't for the guidance, support, mentorship, and encouragement from a number of different people. First, I would like to thank my supervisor Dr. Leyla Soleymani. Her guidance, insight, and encouragement have all been instrumental in the development of this work and my own growth as a researcher. I deeply appreciate the care and concern she had towards my professional development. I would also like to thank my committee members Dr. Thomas Doyle and Dr. Qiyin Fang for their valuable feedback that helped shape the direction of this work.

Thank you as well to the other students in the Soleymani lab. Your profound knowledge could not have been more helpful. I had a tremendous amount of fun with you all both inside and outside of the lab. I would specifically like to thank those that I collaborated with for this work. Thank you Dr. Richa Pandey for providing invaluable shadowing opportunities, experimental assistance, insight, and for responding to hundreds of questions. Thank you Sadman Sakib for presenting me with an opportunity to collaborate and for all your help with paper writing. Thank you Enas Osman for guiding me through some of my first electrochemical experiments and for providing your support on this work. Thank you, Dr. Sudip Saha and Roderick Maclachlan for your insight and integral editing skills.

Lastly, I would like to thank all my loved ones (parents, sister, friends, partner, you all know who you are) for the constant support throughout my masters. Your ability to tolerate countless discussions about device assembly, smartphone application design, and debugging is both impressive and mindboggling. Thank you to my parents for supporting me throughout my years of studies and always having an interest in my work even when you didn't understand it. Finally, thank you to my sister Jessica for putting up with this more than anyone else by virtue of being my roommate.

Chapter 1: Introduction

1.1 Background

From the rapid spread of the ongoing COVID-19 pandemic to the increasing rates of antibiotic resistances[1], a number of recent health crises affecting both humans and animals alike highlight the critical need for accurate and rapid testing. Beyond pathogenic diseases, detection of early-stage cancer biomarkers like prostates specific antigen for prostate cancer[2] and carbohydrate antigen 125 for ovarian cancer[3] for example, are instrumental in increasing patient survivability and improving quality of life. Commonly employed techniques to detect pathogens include cell culturing[4,5], polymerase chain reaction (PCR)[4,5], enzyme-linked immunosorbent assay (ELISA)[4,5], western blot[4,6], and flow cytometry[4,7]. On the other hand, cancer diagnoses often rely on imaging techniques like magnetic resonance imaging and ultrasound[8]. Common among these techniques is their time-consuming nature and reliance on both expensive equipment and trained professionals, rendering them unsuitable for point-of-care (PoC) diagnostics. Accordingly, there is a need for rapid and decentralized diagnostic equipment which can be used to effectively control the spread of diseases and detect early-stage disease biomarkers. Such techniques could lead to more efficient and less expensive diagnostic pathways (Figure 1.1), which can ultimately help clinicians develop disease management strategies in a more timely manner. In particular, there has been growing interest in smartphone operated PoC devices due to their increased computational abilities, connectivity to the internet, and widespread global adoption [9].

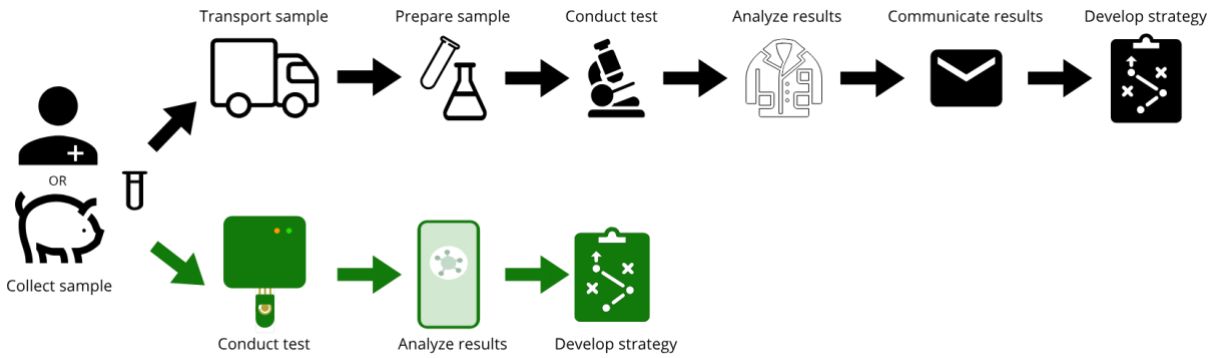

Figure 1.1: Point-of-care versus traditional diagnostic testing. Traditional testing methodologies face significantly more administrative burdens compared to point-of-care.

Electrochemical and photoelectrochemical (PEC) biosensors have emerged as suitable candidates for PoC diagnostics[10,11]. These biosensors pose a number of advantages over other diagnostic techniques. In particular, they are easily miniaturized, inexpensive, rapid, and sensitive[12]. Importantly, the signal output of these biosensors can be used to detect the presence of and determine the amount of target analyte present.

Readout of electrochemical and PEC biosensors is conducted using a potentiostat. Unfortunately, the few commercially available portable potentiostats[13–15] prove to be too costly for many PoC applications and have no means of performing PEC biosensing. While there has been renewed interest in developing low-cost portable potentiostats among researchers, the vast majority of such devices are only compatible with standard two or three-electrode systems for electrochemical biosensing and would accordingly require manual reconfiguration to conduct multiplexed biosensing. Furthermore, some assays are laboratory-bound due to non-trivial sample preparation or signal actuation stages that rely on auxiliary laboratory instruments[16,17]. Accordingly, there is a need for a readout device with non-trivial actuation abilities that can perform multiplexed PoC electrochemical and photoelectrochemical biosensing.

1.2 Objectives

The primary objective of this research is to develop a low-cost electrochemical and PEC readout system to facilitate PoC biosensing. Unlike other similar devices, this readout system should support dual signal assays without the need for manual reconfiguration of the electrodes. In order to perform PoC PEC biosensing, this readout system should interface with, and automatically control an optical excitation source. Due to the portable nature of this device and the low signal amplitude nature of many electrochemical and PEC biosensing experiments, it must be able to account for various sources of noise including 50/60Hz main line noise. To support biosensors with non-trivial processing and actuation requirements, this device will interface with commonly employed peripheral instruments, namely a sample heater and electromagnet. Accounting for the fact that users may be unfamiliar with electrochemical/PEC experimental protocol, this device should be easy to operate. Accordingly, sufficient instructions should be provided to the user, scan parameter configuration should be streamlined, and much of the data processing and analytics performed automatically without the need for manual intervention.

1.3 Outline

This document consists of five chapters. The following is an overview of the remaining four chapters.

Chapter 2 consists of brief literature reviews which familiarizes the reader with topics pertinent to this work. In particular, this chapter reviews the fundamentals of electrochemical and photoelectrochemical biosensing, characterizes the different types of voltammetric techniques supported by this readout system, outlines the sensing principles of DNA and DNAzyme-based biosensors, and dives into the operating principles and development trends of potentiostats.

Chapter 3 focuses on the design and fabrication of a smartphone-operated readout system for point-of-care electrochemical biosensing. Several experiments were conducted to highlight the novelty of this device in comparison to both commercial and other lab-made potentiostats. In addition, the noise characteristics of the device are presented and the readout system is directly compared to a commercially available portable potentiostat.

Chapter 4 elaborates on the modifications made to the aforementioned readout system such that it could support PoC PEC biosensing. Several experiments were conducted to highlight the versatility and applicability of this PEC reader. In addition, the performance of this device is compared to a commercially available PEC workstation.

Chapter 5 summarizes the key findings of this thesis. The contributions to the field and proposed future work are also discussed.

Chapter 2: Literature Review

2.1 Preface

The purpose of this chapter is to review key background information that is pertinent to the understanding of this work. First, an overview of the different sensing techniques employed in subsequent chapters is provided. Specifically, the principles of electrochemical and photoelectrochemical biosensing are presented and the different types of voltammetric techniques supported by this readout system are detailed. Following this, a review of the specific biorecognition elements employed in this work is provided. Lastly, the working principles of electrochemical/PEC readout systems are outlined and device development trends as reported in the literature are presented. This is done to highlight key differences in terms of both design and performance between other devices and the readout system presented herein.

Multiple authors have contributed to the *Review of Specific Biorecognition Elements* section of this chapter, as it has been prepared for submission as part of a broader literature review with the working title "A systemic review of the DNAzyme based electrochemical biosensors for human health: Advancements towards clinical applicability" in the sensors section of the Journal of The Electrochemical Society. Dr. Richa Pandey was the primary author of this section. Enas Osman and Alexander Scott contributed to the writing and editing. Dr. Leyla Soleymani contributed to the design and writing of this section. All other sections of this chapter were independently written by Alexander Scott. Edits were provided by Roderick Maclachlan.

2.2 Introduction to Electrochemical and Photoelectrochemical Biosensing

Electrochemical biosensors

Electrochemical biosensors have received significant attention in recent years as they are rapid, highly sensitive, easily miniaturized, and provide a straightforward relation between the flow of electrons and the biochemical reaction occurring at the electrode[18,19]. Importantly, electrochemical biosensors can be used to detect the presence and quantify the amount of bio-analyte present in a

solution[20]. Popular electroanalytical methods include electrochemical impedance spectroscopy (EIS) and voltammetry. In EIS, AC voltages of varying frequencies are applied to the electrochemical cell and using equivalent electrical circuit models, the impedance of the electrochemical cell can be interpolated[21]. This provides insight into the charge transfer and diffusion of reactants[22]. Conversely, in voltammetry the voltage applied to the electrochemical cell is varied as a function of time and the current generated through the resulting redox reaction is measured. Voltage is plotted against time to create voltammograms, graphical representations of the output of voltammetric scans. In many electrochemical methods, a three-electrode system is used [23]. This consists of a reference electrode (RE), counter electrode (CE), and a working electrode (WE) on which the biorecognition element is surfaced immobilized[23]. Importantly, the WE should be composed of a material that is redox-inert at the applied potential range since the electrochemical interaction of interest occurs on the surface of the WE[24]. The CE completes the electrochemical circuit and allows for current to flow through the electrochemical cell in order to compensate for the redox reaction occurring at the WE[24]. This electrode is typically made of a conductive and inert material like platinum[24]. Lastly, the RE provides a well-defined stable potential such that the potential at the WE can be measured against[24]. Saturated calomel electrode (SCE), standard hydrogen electrode (SHE), and Ag/AgCl electrodes are commonly used as reference electrodes[24].

The defining characteristics of voltammograms like the peak current, peak voltage, and general signal shape can be attributed to the combined effect of the Nernst equation and Fick's laws[24,25]. In accordance with the Nernst equation (Equation 2.1), the potential of the electrochemical cell influences the concentration of the redox species and the relative rate of oxidization and reduction[24,25]. Fick's first law (Equation 2.2) relates the flux of a material to the concentration gradient and diffusion coefficient. Fick's second law (Equation 2.3) is used to determine the rate of change in concentration of a species as a function of time. Accordingly, this transportation of the

redox species controls the rate of reaction at the surface of the working electrode and explains the generation of a diffusion layer[24,25].

(2.1)

$$E = E^0 + \frac{RT}{nF} \ln \frac{[Ox]}{[Red]}$$

Where:

- **E = the potential of the electrochemical cell**
- **E^0 = the standard potential**
- **R = the universal gas constant**
- **T = temperature**
- **n = number of electrons**
- **F = Farraday Constant**

(2.2)

$$J_O = -D_O \frac{\partial c_O}{\partial x}$$

Where:

- **J = diffusion flux**
- **D = diffusion coefficient**
- **$\frac{\partial c_O}{\partial x}$ = concentration gradient of the redox species**

(2.3)

$$\frac{\partial c_O}{\partial t} = -\frac{\partial^2 c_O}{\partial x^2}$$

Where:

- **$\frac{\partial c_O}{\partial t}$ = rate of change of concentration**
- **D = diffusion coefficient**
- **$\frac{\partial^2 c_O}{\partial x^2}$= curvature of the concentration profile**

Photoelectrochemical biosensors

PEC experiments, much like electrochemical experiments, require a potentiostat for readout purposes and a cell consisting of a suitable electrolyte, RE, CE, and WE on which the

biorecognition element is surface-immobilized. However, unlike in electrochemical experiments, PEC experiments make use of an optical excitation source and the WE must be composed of a photoactive material. Light is absorbed by the photoactive WE, resulting in the generation of electron and hole pairs, the subsequent charge transfer of the WE, and the generation of a photocurrent between the WE and CE[11]. This decoupling of the excitation source from the sensing modality grants PEC biosensors with high sensitivity and a low background signal[11,26].

Target analyte recognition events lead to changes in the photocurrent level. Signal-on assays enhance the photocurrent whereas signal-off assays decrease the photocurrent[27]. By comparing the photocurrent levels pre and post-target incubation, the amount of target analyte can be effectively quantified[11].

Voltammetry

Voltammetric methods include square wave voltammetry, differential pulse, normal pulse, linear sweep, cyclic voltammetry, and chronoamperometry. Figure 2.1 is provided to illustrate the different types of voltammetric excitation signals and the resulting current responses.

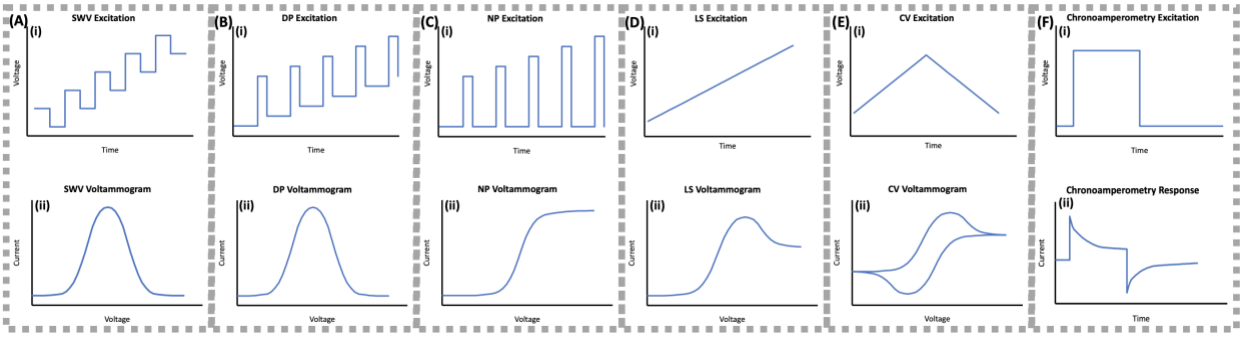

Figure 2.1: Illustrative representations of different excitation waveforms (i) and current response (ii) for (A) square wave voltammetry (SWV), (B) differential pulse (DP), (C) normal pulse (NP), (D) linear sweep (LS), (E) cyclic voltammetry (CV) and (F) chronoamperometry.

Square wave voltammetry (Figure 2.1A) is a small amplitude pulse technique whereby a symmetrical square wave is superimposed on a staircase waveform[28]. The current reading is a differential measurement wherein the current measured at the end of the return pulse — known as the reverse current — is subtracted from the current measured at the end of the forward pulse — known as the forward current[28]. Importantly, the peak current is proportional to the concentration of the analyte[28]. Square wave voltammetry is known for its rapid response time, high sensitivity, and ability to suppress non-Faradaic background current[29].

In differential pulse voltammetry (Figure 2.1B), short amplitude potential pulses are superimposed on a base potential which is incremented/decremented by a step potential at the end of each pulse[29]. The resulting current is the differential measurement of the current at the end of the pulse and the current immediately prior to the pulse. Much like in square wave voltammetry, this differential measurement minimizes the impact of capacitive current, allowing for more sensitive measurements when compared to linear sweep techniques[29].

In normal pulse voltammetry (Figure 2.1C), pulse potentials of a set duration and increasing amplitude are superimposed on top of a DC potential and the current is sampled at the end of each pulse[28]. Normal pulse voltammetry is primarily used in experiments wherein the stability of the WE surface is paramount since in this technique the electrode surface returns to its initial conditions at the end of each pulse[28].

In linear sweep voltammetry (Figure 2.1D), the potential is linearly swept as a function of time. In so doing, a redox reaction occurs at the surface of the WE. Initially, little current is generated; however, faradaic current is generated as the sweep progresses. The amount of current generated rapidly increases until the peak current is recorded at which point the current begins to decrease. This property is the result of the increase in electron transfer in conjunction with the development of a diffusion layer at the surface of the working electrode[24,30,31].

The cyclic voltammetry excitation waveform (Figure 2.1E), much like that of linear sweep, involves the linear sweeping of potential as a function of time[30]. As the potential is swept towards the end potential, current will flow, oxidizing or reducing the analyte depending on the polarity of the sweep[30]. However, unlike linear sweep, once the end potential is reached, the potential is then swept in the opposite direction[30]. In so doing, the analyte is either oxidized or reduced in opposition with the previous sweep[30]. Cyclic voltammetry is widely used as it provides information about the reversibility of the redox reactions and electrochemical kinetics[24,30]. It should be noted that due to their similarities, cyclic voltammetry can generally be used in place of linear sweep.

Unlike the previous methods, in chronoamperometry current is measured as a function of time[32]. The WE is initially held at a potential that does not lead to a redox reaction and is later stepped to a large final potential that mediates the generation of current[33]. In many applications, the potential may be stepped back to the original value after a certain amount of time has passed[33]. It should be noted that chronoamperometry is one of the slowest voltammetric techniques because sufficient time must pass in order to minimize the impact of electrode charging capacitance current[32]. Another key limitation of chronoamperometry is that it is not selective[32]. This is because the applied step potential is sufficiently large enough to reduce/oxidize multiple species in the solution. In a subsequent chapter of this work, we employed a modified version of chronoamperometry for PEC biosensing wherein the potential is kept constant and the current is measured as a function of time while an optical excitation source is toggled OFF and ON.

2.3 Review of Specific Biorecognition Elements

There exist various types of biorecognition elements that specifically interact with an analyte of interest through different types of biochemical mechanisms[34]. This includes enzymes[35,36] nucleic acid[37–40], functional nucleic acids like DNAzymes[41–43], aptamers[44,45], and other proteins[46–48]. In this work, both DNA and DNAzyme based biosensors are used.

Accordingly, in this section, an overview of the operating principles of these two biorecognition elements is presented.

As a molecule, DNA is inherently more stable than proteins. It can be easily synthesized and chemically modified. It is stable over extended periods of time, and it has predictable and programmable features. One of the biggest advantages of using DNA-based probes — typically short oligonucleotides — for molecular recognition and signal transduction is the inherent electrochemical properties of DNA[49–51]. DNA can be immobilized on the surface of an electrode, and by this mechanism, changes in the secondary structure of the DNA, hybridization state of the DNA, or interactions of the DNA with target analytes can lead to changes in the electrical properties of the DNA[49]. DNA can also be labeled with redox moieties, adding complexity oftentimes resulting in increased specificity, to the device[49,50]. Additionally, the negatively charged backbone of the DNA allows for its interaction with electroactive molecules, whereas other electroactive molecules preferentially interact with double versus single-stranded states (i.e., groove binders or intercalators which interact with double-stranded DNA).

Investigations into the functional capacity of nucleic acids were propelled forward in the late 1980s, significantly by the parallel work of Sidney Altman and Thomas R. Cech. Their work demonstrated that RNA was capable of catalytic behaviour[52]. Consequently, the early 1990s saw the development of *in vitro* selection methods to identify synthetic catalytic RNA molecules (ribozymes) as well as both RNA and DNA affinity ligands (aptamers)[53–56]. Only five years after the seminal discovery of naturally occurring Ribozymes, synthetic DNAzymes which could cleave RNA were described by Breaker and Joyce[57]. Since then, there has been rapid growth in the field of functional nucleic acids (FNAs) with the development of DNAzymes[58–62].

DNAzymes have been widely applied to the field of biosensing due to their dual role in molecular recognition and signal transduction, which can be designed for during *in vitro* selection. RNA-cleaving DNAzymes catalyze the intra- or intermolecular cleavage of a single ribonucleotide site generating an oligonucleotide fragment which can be used for signal transduction in diverse assays. RNA-cleaving DNAzymes can be derived either directly or indirectly by an iterative in vitro selection process. In general, DNAzymes can be easily modified to include internal or terminal modifications (i.e., fluorophores, quenchers, nanoparticles, reactive functional groups). They are relatively inexpensive to synthesize, and experience little-to-no batch-to-batch variation. *In vitro* selection begins with a library of partially randomized oligonucleotides. The library is prepared with two known primer regions that flank a centralized random region of a fixed length. RNA-cleaving DNAzymes also feature the addition of a known substrate region to the 5'-end of the template sequence. During the first essential step, the selection library is incubated with a target molecule or samples derived from a target organism (such as bacteria). For example, the library may be incubated with either a specific protein, small molecule, or the crude extracellular mixture obtained from a bacterial culture. Following incubation, the library is screened for library sequences that are activated by the targets. For RNA-cleaving DNAzymes, those undergoing a cleavage reaction in the presence of the target molecule are maintained, and those that remain intact are partitioned away. This is often achieved by gel electrophoresis, where the cleaved (active) portion of the selection library migrates at a different rate than the intact (inactive) portion of the selection library and is therefore physically separated. Following this partitioning step, active sequences are amplified by polymerase chain reaction using the pre-designed region, to obtain an enriched library in preparation for another round of selection. Through this iterative process, sequences that are highly active and selective are identified. Typically, multiple rounds

of selection are required[63–65] with an average of 15 ± 4 rounds reported for bacterium-specific RNA-cleaving DNAzymes[60].

DNAzyme-based electrochemical biosensors are categorized as label-free, labelled, or bio-barcode assays. In label-free assays, target binding changes the structural configuration of the DNAzyme caused by cleavage or the formation of the secondary-tertiary structures. This structural change reduces the access of redox reporters to the electrode surface in signal-off assays or increases the diffusion of the redox reporters in signal-on assays. In labelled assays, the DNAzyme is tagged with a redox moiety capable of generating an electrochemical signal. In labelled signal-on assays, target capture brings the redox label to the electrode proximity; whereas in signal-off assays, the redox label is released from the electrode surface. In bio-barcode assays, target capture is first translated to the release of a barcode analyte such as small redox molecules or redox-tagged oligonucleotides, which is followed by the detection of the barcode at the electrode surface.

2.4 Operating Principles of Potentiostats and a Review of Potentiostats Reported in the Literature

Central to electrochemical and PEC biosensing is the potentiostat, which provides means of controlling the potential of the cell and reading the resulting current. The three-electrode potentiostat was originally developed by Archi Hickling — an electrochemist at the University of Leicester — so that the potential of the WE could be set to any desired value[66]. Early versions of potentiostats were large analog instruments and were accordingly confined to laboratory settings. The rise of digital electronics and improvements in integrated circuit manufacturing in the 1980s led to significant changes in potentiostat design. In particular, this enabled potentiostats to connect to computers so that measurements could be saved and the data processed[67]. Building upon this, significant effort has been made in recent years to improve the portability of potentiostats in order to facilitate away-from-lab biosensing[9].

A simplified representation of a potentiostat can be found in Figure 2.2. This design makes use of three different operational amplifiers. At the output of the WE sits a transimpedance amplifier (TIA), which converts the current output of the cell into a voltage so that the measurement can be processed by digital components[68]. Importantly, this component draws little current so as to not impact the conversion[68]. A measurement resistor sits in parallel with a stabilizing capacitor, which is added to prevent oscillatory behaviour, to form a negative feedback loop. Real world operational amplifiers introduce input capacitance. This, in conjunction with the fact that the TIA provides unity gain due to the large resistance of the electrochemical cell relative to the feedback resistor, means that the TIA is unstable without the introduction of the feedback capacitor. The current measurement range of the potentiostat is dictated by the value of the feedback resistor and the output of the TIA is calculated in accordance with equation 2.4. The transfer function of the TIA is shown in equation 2.5. Using equation 2.6, an appropriate feedback capacitor can be selected to prevent oscillations and ensure stable performance of the operational amplifier.

(2.4)

$$V_{out} = -I_{cell} R_f$$

Where:

- $\boldsymbol{V_{out}}$ **= the output voltage of the TIA**
- $\boldsymbol{I_{cell}}$ **= the current entering the TIA through the electrochemical cell**
- $\boldsymbol{R_f}$ **= the feedback resistor**

(2.5)

$$\frac{V_{out}}{I_{cell}} = \frac{-R_f}{1 + sR_f C_f}$$

Where:

- V_{out} = **the output voltage of the TIA**
- I_{cell} **= the current entering the TIA through the electrochemical cell**
- R_f**= the feedback resistor**
- C_f**= the feedback capacitor**

(2.6)

$$C_f = \sqrt{\frac{C_{in}}{2\pi * R_f * GBW}}$$

Where:

- C_f**= the feedback capacitor**
- C_{in}**= the input capacitance of the TIA**
- R_f**= the feedback resistor**
- **GBWP= the gain bandwidth product of the TIA**

The RE connects to the positive terminal of a voltage follower (VF) to isolate the RE. This ensures that no current will be drawn from the RE, allowing it to act as a stable reference. Lastly, a control amplifier (CA) injects current into the electrochemical cell to compensate for the redox reaction occurring on the WE and to maintain the potential difference between the WE and RE.

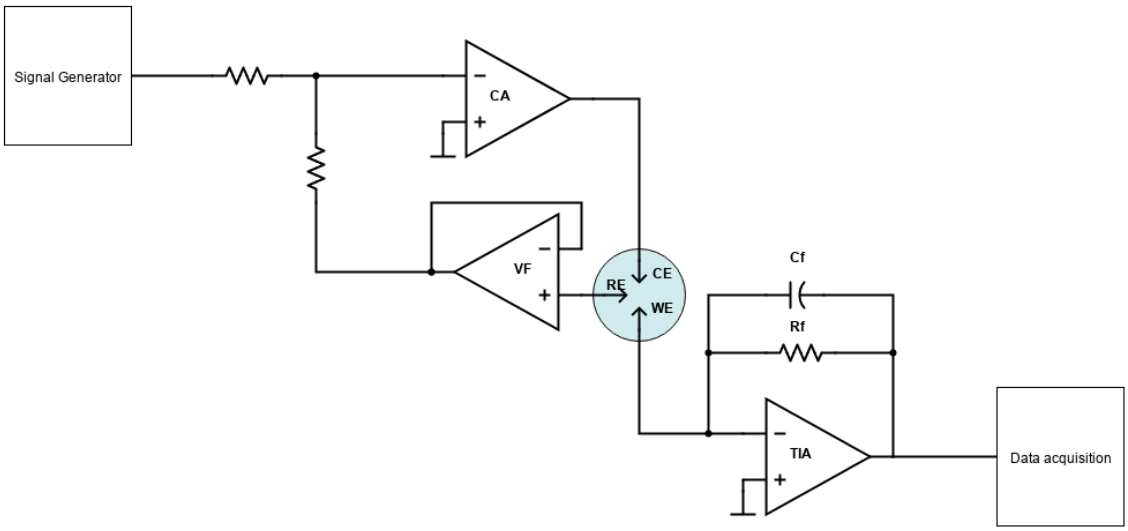

Figure 2.2: Simplified potentiostat circuit consisting of a signal generation unit, control amplifier (CA), voltage follower (VF), transimpedance amplifier (TIA) with a feedback resistor and capacitor in parallel, and a data acquisition system.

In recent years, a number of lab-made potentiostats have been developed that are less costly and more portable than commercially available potentiostats. For the remainder of this section, these lab-made potentiostats will be categorized based on their main objectives and key limitations. Noteworthy examples of each will be highlighted. Provided in Table 2.1 is a comparative summary of commercially available and select laboratory-made potentiostats including the reader developed herein.

Table 2.1: Comparison of Select Potentiostats

Potentiostat	**Price (USD)**	**Dimensions WHD (mm^3)**	**Weight (g)**	**Supported Techniques**	**PEC**	**Connectivity**
Sensit Smart[14]	>700	43 x 11 x 25	10	LS, CV, SWV, DP, NP, CA, CC, MA, PAD, OCP, EIS	No	USB-C (phone, computer)
Palmsens 4[13]	>5,000	157 x 35 x 97	~500	LS, CV, ACV, SWV, DP, NP, CA, ZRA, CC, MA, FAM, PAD, MPAD, LSP, CP, MP, OCP, SCP EIS	No	Bluetooth, USB (phone, computer)
µStat-i 400[15]	>5,000	100 x 36 x 132	540	LS, CV, ACV, SWV, DP, NP, CA, ZRA, CC, MA, FAM, PAD, MPAD, LSP, CP, MP, OCP, SCP EIS	No	Bluetooth, USB (computer)
Zahner CIMPS-QE/IPCE[69]	>10,000	Electronic load: 470 x 160 x 446 Potentiostat: 364 x 160 x 376	Electronic load: 20,000 Potentiostat: 12,000	LS, CV, ACV, DP, CA, MA, CP, EIS, among other PEC specific techniques	Yes	USB (computer)
UWED[70]	~60	80 x 23 x 40	56	LS, CV, SWV, DP, CA, CP	No	Bluetooth (phone)
DStat[71]	~100	92 x 31 x 84	~100	LS, CV, SWV, DP, CA, CP	No	USB (computer)
Cheapstat[72]	<80	140 x 28 x 66	115	LS, CV, SWV	No	USB (computer)
Enactsense / PECsense (this work)	~100	75 x 15 x 45 with case excluding battery	50 with case excluding peripheral devices and battery	LS, CV, SWV, DP, NP, CA	Yes	Bluetooth (phone)

LS- Linear sweep; **CV**- cyclic voltammetry; **ACV**- AC voltammetry; **SWV**- square wave voltammetry; **DP**- differential pulse; **NP**- normal pulse; **CA**- chronoamperometry; **ZRA**- zero resistance amperometry; **CC**- chronocoulometry; **MA**- multistep amperometry; **FAM**- fast amperometry; **PAD**- pulsed amperometric detection; **MPAD**- multiple-pulse amperometric detection; **LSP**- linear sweep potentiometry; **CP**- chronopotentiometry; **MP**- multistep potentiometry; **OCP**- open-circuit potentiometry; **SCP**- stripping potentiometry; **EIS**- electrochemical impedance spectroscopy

Educational Potentiostats

Motivated by the numerous real-world applications of electrochemical detection, several research groups have designed low-cost potentiostats to be used as educational tools to help familiarize students with the fundamentals of these techniques[72–75]. These potentiostats follow a

do-it-yourself approach and are composed of common, inexpensive electrical components. While these devices are markedly inexpensive (20-80 USD), they may not be suitable for all biosensing experiments given their low current sensing resolution and large excitation signal quantization error. Regardless, they highlight the growing need for low-cost potentiostats outside of a traditional research laboratory setting.

Gabriel Meloni fabricated a low-cost (<30 USD) potentiostat for performing cyclic voltammetry using standard "off the shelf" electrical components designed for students to learn the fundamentals of electrochemistry[75]. This potentiostat uses an 8-bit DAC and the excitation potential range is limited to ±1V, resulting in an excitation signal resolution of 0.0078V. A single feedback resistor was used to yield a current measurement range of ±200μA. A 10-bit ADC was used and accordingly, the current sensing resolution of this device is 0.4μA. Another noteworthy example is Cheapstat, which was developed by Aaron Rowe and colleagues at the University of California Santa Barbara in 2011[72]. This open-source, inexpensive (<80USD), and portable potentiostat laid the groundwork for other portable potentiostats to come. This potentiostat uses a 12-bit DAC and the excitation potential range is limited to ±1V, resulting in an excitation signal resolution of 0.49mV. Cheapstat offers two current measurement ranges by toggling between two different feedback resistors (±10μA and ±100μA). By using a 12-bit ADC, the current sensing resolution of Cheapstat is 0.0049μA and 0.049μA for the ±10μA range and ±100μA range respectively. By connecting to a desktop computer and using the graphical user interface, users can select between cyclic, square wave, linear sweep, and anodic stripping voltammetry. Using this program, the voltammograms can be plotted, but it does not include any signal processing or analytical abilities.

Computer-Controlled Potentiostats

As an alternative to the expensive commercially available potentiostats, many researchers have developed general-purpose, low-cost potentiostats to be used within a laboratory setting[68,72,76–79]. Compared to the previously mentioned education-centric devices, these potentiostats offer improved performance but are accordingly more expensive (50-200 USD). However, these devices have limited application in PoC settings given their reliance on a computer for data analysis. This proves to be a significant hurdle particularly in resource-limited environments given the added equipment cost and electricity dependence. Furthermore, many of these devices are controlled by highly technical software with advanced settings. Despite this, the analytical capabilities of these devices are limited as they do not include analytical algorithms found standard in the commercial systems.

One of the most notable computer-controlled potentiostats reported in the research literature is DStat, an open-source potentiostat developed by Michael Dryden and Aaron Wheeler at the University of Toronto in 2015[71]. This potentiostat is of particular interest as it offered significantly improved performance when compared to the previously mentioned Cheapstat while remaining cost-effective (~100 USD). This potentiostat uses a 16-bit DAC and the excitation potential range is limited to ±1.5V, resulting in an excitation signal resolution of 46μV. Seven feedback resistors are used in conjunction with a 24-bit ADC, with a limit of detection of 600fA in the lowest current measurement range. The open-source nature of this device meant that researchers could revise the hardware or expand upon the functionality of the device through software modifications.

Smartphone-Operated Potentiostats

In an effort to create more portable readout systems, some researchers have developed smartphone-operated potentiostats[70,80–83]. Most of these devices communicate with the smartphone via wireless protocols [70,80–82], although some rely on physical connections to the smartphone[83]. These smartphone-operated potentiostats are comparatively priced to the computer-controlled potentiostats and are inherently better suited for PoC biosensing given the ubiquity and portable nature of smartphones. Unfortunately, most of these smartphone applications provide little user interface beyond simply presenting the scan measurements in voltammogram format. Analytical functions such as data smoothening, peak detection, and classification algorithms remain unincorporated within these applications. Furthermore, while these smartphone-operated potentiostats have an away-from-lab focus, their inability to interface with and control other biosensing instruments renders any biosensor with such requirements dependent on other traditionally laboratory-bound external equipment.

A prime example is the Universal Wireless Electrochemical Detector (UWED) developed by Alar Ainla and colleagues in 2018[70]. This potentiostat was one of the first open-source smartphone-operated potentiostats reported in the research literature. This potentiostat is controlled wirelessly via BLE by an accompanying smartphone application. Collected scan data is transferred from UWED to the smartphone and subsequently uploaded to the Cloud. Given this reliance on the Cloud, UWED offers little in terms of signal processing in-app when compared to portable commercial systems. This potentiostat uses a 16-bit DAC and the excitation potential range is limited to ±1.5V, with a reported excitation signal resolution of 67μV. A single feedback resistor grants this potentiostat a current measurement range of ±180μA range. By using a 16-bit ADC, the current sensing resolution of this device is 6.4nA barring any input-referred noise.

Chapter 3: A Portable and Smartphone Operated Electrochemical Reader and Actuator that Streamlines the Operation of Electrochemical Biosensors

3.1 Preface

The purpose of this chapter is to demonstrate the design and validation of a portable electrochemical readout system. The limitations associated with existing electrochemical readout systems are discussed. The design of the readout system is outlined. Experiments were conducted to validate the sensing abilities of the device, highlight its ability to control portable auxiliary instruments, and demonstrate its applicability with differential signal assays.

Multiple authors have contributed to this chapter as it has recently been prepared for publication with the working title of "A Portable and Smartphone Operated Electrochemical Reader and Actuator that Streamlines the Operation of Electrochemical Biosensors" in the Journal of Analytical Chemistry. Enas Osman was responsible for preparing the DNA used in the electrochemical experiments. Alexander Scott was responsible for designing the hardware and developing all software associated with the electrochemical readout system. Alexander Scott conducted the electrochemical and electrical demonstration experiment, the sample heater validation using a 3-electrode bio-barcode assay experiment, and the magnetic manipulation validation experiment. Both Alexander Scott and Dr. Richa Pandey performed the two-channel electrochemical differential detection of Escherichia coli experiment. Alexander Scott wrote this article. Enas Osman wrote the *DNAzyme synthesis and purification* and the *Preparation of crude intracellular matrix* subsections in the Methods and Materials method section of this work. Dr. Richa Pandey contributed to editing. In addition, Dr. Leyla Soleymani contributed to the design and writing of this section.

3.2 Introduction

Since the commercialization of the first glucose biosensor in 1975[84], there has been tremendous interest in using electrochemical readout for disease management and health

monitoring at the point-of-care (PoC). A number of electrochemical biosensors, which combine biorecognition elements with electrochemical transducers, have emerged in the research literature for detecting pathogens[20] , extracellular vesicles[85], biomolecules[10,86], and small molecules[87]; however, none of these classes of biosensors have penetrated the market to the same degree as PoC glucose monitors[88]. Issues related to sensor stability, trade-offs between assay time, sensitivity, and complexity, loss of performance in clinical samples, and integration challenges[89] are all contributing factors to the difficulty in translating electrochemical biosensors from the laboratory to commercial markets. In the context of integration, it remains challenging, costly, and time consuming to adapt commercially-available electrochemical readers, postentiostatic or galavaostatic devices referred to generally as potentiostats, for use with specific PoC biosensors. In particular, commercially available potentiostats are prohibitively expensive and pose a number of developmental challenges for PoC analysis given their generally large size (although miniaturized potentiostats are becoming increasingly common[14]), difficulty in use and data interpretation by non-experts, and perhaps *most importantly* their lack of actuation abilities needed for evaluating certain biological assays. A vast number of bioassays require sample heating, magnetic manipulation, and multiplexed measurements, which are typically performed using devices separate from the potentiostat, posing significant integration challenges.

In response, a number of lab-made potentiostats have been reported in the literature in recent years[68,72,73,76–82,90–99]. While these devices are less costly than their commercial counterparts, they do little to address other key integration challenges that inhibit many electrochemical biosensors from penetrating the market. Many of these lab-made devices rely on a connection to a computer[68,76–79,96,100], which may not be feasible in all PoC applications,

particularly in resource-limited environments. Others rely on highly technical software that is tailored to researchers, providing little instructions to the user. In addition, little work has been done to incorporate the aforementioned actuation instruments despite their incorporation in a number of electrochemical biosensing experiments[101]. Lastly, both the commercial systems and the devices reported in the literature are designed for use with standard 2-electrode or 3-electrode systems and are therefore incompatible with multi-channel and multiplexed assays[43].

As such, the aim of this work was to develop a fully-integrated handheld electrochemical platform that combines dual channel (can be extended to multiple channels) signal readout with sample processing and signal actuation to expedite the translation of bioassays from the laboratory to the market. More specifically, this device can perform *away-from-lab* sample heating and magnetic manipulation. This device was thoroughly characterized by performing various electrochemical techniques and it was further validated using a two-working electrode biosensing assay which integrates electroactive DNAzymes with electrochemical readout for bacterial detection, thereby demonstrating the feasibility of the platform in a real-time PoC analysis capacity.

3.3 Materials and Methods

Reagents and Materials

Escherichia coli K12 (*E. coli K12; MG1655*), which is regularly maintained in our laboratory, was used in this study. Lyophilized oligonucleotides were purchased from Integrated DNA Technologies, Inc (Iowa, United States). Methylene blue N-Hydroxysuccinimide (NHS) ester was purchased from Glen Research (Virginia, United States). Dimethyl sulfoxide (DMSO), sucrose, xylene cyanole FF, bromophenol blue, 10X tris-borate-EDTA buffer (TBE), tris, ethylenediaminetetraacetic acid (EDTA), Sodium Acetate, Glacial Acetic Acid, and sodium

chloride was purchased from Sigma-Aldrich (Ontario, Canada). Urea, and 40% 29:1 bis/acrylamide was purchased from Bioshop Canada (Ontario, Canada). A Stuart handheld ultraviolet (UV) lamp 254/365 nm was purchased from Cole-Parmer (Ontario, Canada). 0.2µm filter discs were purchased from Acrodisc. The shaker (76407-108) was purchased from VWR (Ontario, Canada). BTV-AC1 electrochemical sensors (referred to here on as on-chip electrodes) were purchased from Palmsens BV (Netherlands). Magnetic beads, which are regularly maintained in our laboratory, were used to demonstrate our system's capability of performing basic magnetic manipulation. All other chemicals were purchased from Sigma-Aldrich and were used without further purification. The specific DNA sequences used in this work can be found in SI Table 3.1.

Device Engineering

The device presented in this work, referred to here on as Enactsense (electrochemical actuator and sensing device), was designed around the low amplitude signal constraints associated with typical biosensing experiments and is capable of performing several types of voltammetric functions (Appendix 3.1). Enactsense is controlled via an Android application through Bluetooth Low Energy (BLE) rather than a dedicated program on a desktop computer, thereby capitalizing on the widespread global adoption, increasing processing power, and the decreasing cost of smartphones, and also rendering the system more portable and accessible. A summary of the device's capabilities can be found in SI Table 3.2.

Device schematics and printed circuit boards (PCBs) were designed using Autodesk Eagle. PCB manufacturing was conducted by JLCPCB and the individual components were hand-soldered. Enactsense is composed of the Arduino Nano 33 BLE development board, the MAX5217 digital-to-analog converter (DAC), a reconstruction filter made of the AD8656 dual

operational amplifier, a core potentiostat circuit consisting of the AD8606 dual operational amplifier and the LMP7721 precision operational amplifier, the ADS122C04 analog-to-digital converter (ADC), and the dual output REF2030 voltage reference.

Novel to Enactsense is the incorporation of peripheral devices that expand upon the device's capabilities. A custom sample heater circuit was developed to facilitate away from lab sample heating. A 3D printed case made of polylactic acid was designed using Autodesk Inventor and printed using an Original Prusa i3 MK3S 3D printer to house an adhesive flexible polyimide heater. This heater was made by Icstation and was purchased through Amazon Canada. The KS0320 Keyestudio Electromagnet Module was also integrated to facilitate away-from-lab magnetic manipulation and was purchased through Amazon Canada.

We developed the firmware using the Arduino integrated development environment and it is responsible for computing the voltammetric excitation series, reading the resulting output from the electrochemical cell, controlling the peripheral devices, configuring the settings of the various integrated circuits, and communicating with the smartphone. The ArduinoBLE external library was used to simplify BLE communications. Sparkfun's ADS122C04 Arduino library was used to interface with the ADC and properly configure its registers. Individual functions were created for each of the supported voltammetric scan types.

We developed an accompanying smartphone application in Java using the Android Studio integrated development environment. This application is responsible for remotely controlling Enactsense, providing means of user interface, and performing any necessary signal processing and analysis. The BlessedBLE library[102] was used to facilitate communication with Enactsense. The voltammetric scans are presented in graphical format using the open-source

MPAndroidChart graphing library[103]. In-app data smoothening was conducted using Marcin Rzeźnicki's open-source SGFilter Java class[104].

Electrical and Electrochemical Characterization

To quantitatively assess the noise performance of Enactsense, the device's electrode connections were left open, and the current was measured in a typical laboratory environment for 7 minutes in order to measure the input-referred noise of the current sensing portion of Enactsense (transimpedance amplifier and ADC). The ADC sampling rate was set to 20 samples per second (SPS). No efforts were taken to shield the device from any forms of interference.

Subsequently, the redox behavior of $[Fe(CN)_6]^{4-}$/ $[Fe(CN)_6]^{3-}$ was investigated at various concentrations and scan rates. On-chip electrodes were cleaned by performing 30 cyclic voltammetry scans with 0.5M sulfuric acid from 0 – 1.5V in 0.001V steps with a scan rate of 0.1V/s using a commercial potentiostat. Following this, 2 mM, 1 mM, 0.5 mM, 0.25 mM, and 0 mM of the $[Fe(CN)_6]^{4-}$/ $[Fe(CN)_6]^{3-}$ solutions were prepared in 25 mM phosphate buffer saline (PBS) and 25 mM NaCl buffer (25:25 buffer). 40µL drops of the solutions were individually pipetted onto the on-chip electrodes following washing with deionized water. Cyclic voltammetry was then performed for a potential range of -0.2V – 0.5V, with steps of 0.001V and a scan rate of 0.2V/s. Subsequently, 40µL drops of the 2mM $[Fe(CN)_6]^{4-}$/ $[Fe(CN)_6]^{3-}$ solution prepared in 25:25 buffer were pipetted onto new on-chip electrodes. Cyclic voltammetry was then performed from -0.2V – 0.5V, with steps of 0.001V and scan rates of 0.2V/s, 0.1V/s, 0.05V/s, and 0.025V/s. In-app data smoothening was not performed. The performance of Enactsense was compared to the commercially available Sensit Smart.

Peripheral Devices Validation

The performance and characteristics of the sample heater and electromagnet were investigated. After first allowing the sample heater to pre-heat for one minute, an on-chip electrode was placed inside the sample heater for 30 minutes. The surface temperature of the on-chip electrode was then recorded every 5 minutes using the SOVARCATE 960 infrared thermometer. Following this, new on-chip electrodes were cleaned by performing 30 cyclic voltammetry scans with 0.1M sulfuric acid from 0 to 1.5V in 0.001V steps with a scan rate of 100mV/s using a commercial potentiostat. A mixture of 1µM tris(2-carboxyethyl)phosphine (TCEP) (1:100) and 1µM probe was prepared in 25 mM phosphate buffer saline (PBS), 25 mM NaCl, and 100mM $MgCl_2$ buffer 25:25:100 solution. After allowing this mixture to stabilize following a 2-hour incubation at room temperature, 3µL drops of the mixture were pipetted onto the on-chip electrodes. The on-chip electrodes were then left to incubate at room temperature in a humid environment for 18 hours. Following this incubation period, 3µL drops of 100mM mercapto hexanol (MCH) backfill were pipetted onto the on-chip electrodes and left to incubate for 20 minutes at room temperature. Square wave voltammograms were recorded using Enactsense from 0V to -0.6V in 0.001V steps with a frequency of 60Hz and a pulse amplitude of 0.025V. Subsequently, 10µL of methylene blue tagged target DNA with a concentration of 150nM were pipetted onto half of the on-chip electrodes and 10µL of PMT20 was pipetted onto the remaining on-chip electrodes. The on-chip electrodes were then incubated for 30 minutes at approximately 37°C using the sample heater. Following this incubation, square wave voltammograms were recorded using Enactsense from 0V to -0.6V in 0.001V steps with a frequency of 60Hz and a pulse amplitude of 0.025V. A similar procedure was performed with another set of on-chip electrodes but they were instead incubated at room temperature (RT)

during the target DNA hybridization step. In-app baseline subtraction and data smoothening were performed.

In order to demonstrate Enactsense's ability to control an electromagnet within an electrochemical biosensing context, it was used to isolate magnetic microbeads in a suspension. The electromagnet was turned on and was placed directly beside a rectangular vial containing 14 µL of DI water and 1 µL of magnetic microbeads for 30 minutes.

Evaluation of a Two-Working Electrode Assay

In accordance with the manufacturer protocol, 5'-Amino- modified *E. coli* DNAzyme (D) was labeled using methylene blue NHS Ester diluted in DMSO. The lyophilized DNAzyme was diluted in 0.1 M Carbonate/Bicarbonate buffer (pH 9). Next, the methylene blue NHS Ester was added to the DNAzyme for methylene blue tagging and left to incubate for two hours at room temperature. Subsequently, the DNAzyme was purified using 10% urea 40% 29:1 Bis/Acrylamide page gel. Prior to loading into the gel, an Ethanol precipitation (0.1x Sodium acetate (pH=5.2), 2.5x 100% ethanol) step was performed. The gel was run for 1 hour and the DNAzyme bands were vitalized and cut using UV light (240 nm). Afterwards, the gel was crushed and eluted using an in-house elution buffer (200 mM NaCl, 10 mM Tris pH=7.5, 1 mM EDTA)[105]. The crushed gel was eluted two more times on a heated shaker at 300 rpm at 37°C for 30 minutes. A final ethanol precipitation step was applied. The retrieved DNAzyme was then diluted in RNA/DNA free water for further use.

The crude intracellular matrix (CIM) preparation protocol was adapted from that of Ali and colleagues[105]. *Escherichia coli K12* (MG1655*)* was grown under the appropriate conditions and cultured in lysogeny broth (LB) media overnight until optical density reached OD_{600} ~1.0. Subsequently, 1 mL of each bacterial culture was centrifuged at 10,000g for 10 minutes and the

clear supernatant was discarded. The cells were then suspended in 500µL of 1x reaction buffer (50 mM HEPES, 150 mM NaCl, 15 mM $MgCl_2$, Tween 20 0.01%, pH 7.5). The cell suspension was heated at 90°C for 5 minutes and subsequently left at room temperature for an additional 10 minutes to ensure proper cell lysis. Next, the suspension was centrifuged at 13,000g for 10 minutes. The clear supernatant was then collected and passed through a 0.2µm filter disc. The supernatant was aliquoted and stored at −20°C and was used in DNAzyme cleavage experiments as needed. This CIM supernatant corresponds to ~2 Å~ 10^9 cells/mL.

On-chip electrodes were cleaned by performing 10 cyclic voltammetry scans with 0.1M sulfuric acid from 0 – 1.5V in 0.001V steps with a scan rate of 100mV/s using a commercial potentiostat. Next, 3 µM of thiolated probe (TP) was reduced using 300 µM TCEP (1:100) for 2 hours in the dark at room temperature. Concurrently, 5 µM of thiolated DNAzyme (TD) was reduced using 500µM TCEP (1:100) for 2 hours in dark at room temperature. After this reduction time had passed, 3µL drops of the TP and TD were deposited onto the respective electrodes. The electrodes were then left to incubate at room temperature for 18 hours. Following this incubation period, the on-chip electrodes were washed in 25:25 buffer. 3 µL drops of 100mM MCH backfill were deposited onto the on-chip electrodes and left to incubate for 20 minutes in the dark at room temperature. Square wave voltammetry was performed using Enactsense from 0V to -0.6 V in 0.001 V steps with a frequency of 60 Hz and a pulse amplitude of 0.025 V. Subsequently, a 10 µL solution of the aforementioned 10^6 CFU/ml bacterial CIM were pipetted onto half of the available on-chip electrodes assigned as Electrode 1 and 10 µL of PMT20 was pipetted onto the remaining on-chip electrodes assigned as Electrode 1 on-chip electrodes. These on-chip electrodes were then incubated for 30 minutes at 37°C in a conventional laboratory oven. Following this 30-minute incubation, the solution on top of these

on-chip electrodes were manually transferred to the on-chip electrodes assigned as Electrode 2. The on-chip electrodes assigned as Electrode 2 were then incubated for 30 minutes at 37°C in a conventional laboratory oven. Square wave voltammetry was recorded using Enactsense from 0V to -0.6 V in 0.001 V steps with a frequency of 60 Hz and a pulse amplitude of 0.025 V. In-app baseline subtraction and data smoothening were performed.

3.4 Results

Device Engineering

We developed a miniaturized (75 mm by 40 mm) and inexpensive (~95 USD) electrochemical reader and actuator (Enactsense) and an accompanying smartphone application, specifically made for use with biological assays. The Bluetooth Low Energy (BLE) communication protocol, a recent low-power revision of the traditional Bluetooth communication scheme, is employed so that the smartphone can remotely control Enactsense. Accordingly, we have developed a universal device that can interface with a wide range of smartphones regardless of their make or model.

Enactsense (Figure 3.1A and 3.1B) is composed of the Arduino Nano 33 BLE development board, a digital-to-analog converter (DAC), multiple operational amplifiers, an analog-to-digital converter (ADC), and a voltage reference. We used the Arduino Nano 33 BLE development board as it natively supports BLE communications without the need for an external BLE module. Furthermore, the Arduino Nano 33 BLE development board has a number of programmable input and output channels, which we used to communicate with the DAC, ADC, sample heater, and electromagnet. Finally, this board is compatible with a number of open-source libraries, which facilitated firmware development. Since the Arduino Nano 33 BLE does not output analog voltages, an external DAC was added. Specifically, we utilized the MAX5217

16-bit DAC to convert the signal from the Arduino Nano 33 BLE development board into an analog voltammetric excitation signal, which controls the potential between the reference electrode (RE) and the working electrode (WE). The dual output REF2030 voltage reference is used to set the maximum voltage output of this DAC to 3V. Accordingly, the voltage resolution of the DAC is 46µV, which allows for small step potentials and is in line with many commercial potentiostats[106]. A reconstruction filter follows the output of the DAC in order to attenuate image frequencies, thereby correcting for the staircase effect associated with the discrete nature of DACs and leading to the generation of smooth voltammetric excitation signals. This fourth order filter is made of two AD8656 operational amplifiers and it offers 0dB gain in the passband with a -3dB frequency of 30kHz, which is suitable given the 100kHz bandwidth of the DAC.

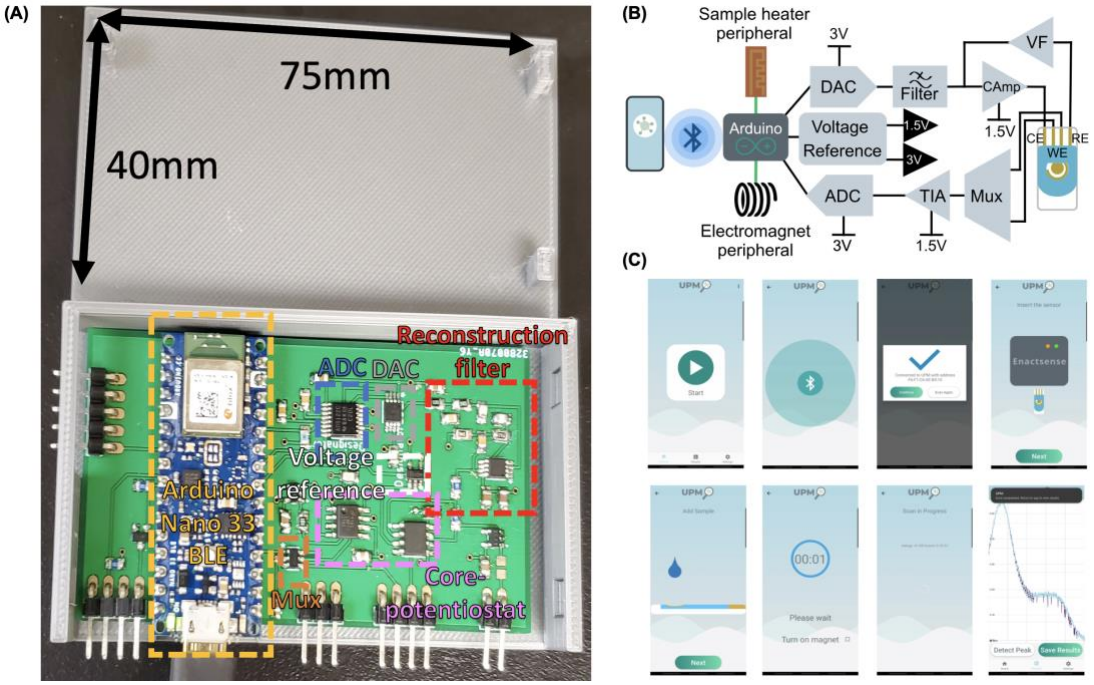

Figure 3.1: Overview of Enactsense. (A) Photograph of Enactsense and a 3D printed case with labels corresponding to the Arduino Nano 33 BLE, digital-to-analog converter (DAC), voltage reference, reconstruction filter, a core-potentiostat circuit consisting of a voltage follower (VF), control amplifier (CAmp), and transimpedance amplifier (TIA), multiplexer (Mux), and an analog-to-digital converter (ADC). (B) Functional block diagram of Enactsense with additional labels highlighting the reference electrode (RE), counter electrode (CE), and working electrodes (WE) and peripherals. (C) Smartphone application process flow.

The core potentiostat circuit, composed of three operational amplifiers, is situated after the reconstruction filter. The first operational amplifier is a voltage follower (VF) which is used to isolate and prevent the flow of current through the RE, thereby ensuring the RE can provide a stable reference. With that said, real-world operational amplifiers do not have an infinite input impedance meaning that an input bias current will still flow through the RE. Next, a control amplifier (CAmp) is responsible for injecting current into the cell to compensate for the redox reaction occurring at the WE. Lastly, a transimpedance amplifier (TIA) converts the current output of the cell into a voltage. The AD8606 dual amplifier was used for the VF and CAmp in part due to its low input bias current (0.2 pA). The small input voltage offset (20 µV) and low voltage noise density (8 $nV/Hz^{1/2}$) of this operational amplifier ensures that the applied potential is accurate. Whereas for the TIA, the LMP7721 was selected chiefly due to its markedly low input bias currents (3 fA), thereby ensuring that the current to voltage conversions are as accurate as possible. In order to support multiplexed measurements as required in many biosensing experiments, we added the MAX4644EUT to toggle the WE that is connected to the input of the TIA. This multiplexer has a switching time of less than 20ns.

Even though the Arduino Nano 33 BLE development board has a built-in 12-bit ADC, the resolution may not provide the level of granularity needed to accurately make diagnostic conclusions. Accordingly, most commercial potentiostats make use of external ADCs with a minimum resolution of 16-bits [106]. As such, we opted to use the external ADS122C04 ADC to convert the voltage output of the TIA into a digital signal that can be recorded by the Arduino Nano 33 BLE and later transmitted to the smartphone. This precision ADC has an effective resolution up to 20-bit dependent on the sampling rate, which can be set from 20 samples per

second (SPS) up to 2000 SPS. The ADS122C04 features a built-in low-pass filter to suppress 50/60 Hz line noise when sampling at 20 SPS.

We have designed Enactsense to interface with a portable heater and an electromagnet to support away-from-lab sample heating and magnetic manipulation. The heater is powered by a separate 12 V power supply and can reach a maximum temperature output of 170℃. The temperature of the sample heater and the magnetic field strength are controlled directly by the Enactsense.

In order to make Enactsense accessible and easy to use, we developed an accompanying Android application that is responsible for connecting to Enactsense, adjusting the voltammetric scan parameters, guiding the user through an experiment, signaling Enactsense to begin a measurement, and displaying the results (Figure 3.1C). We employed the BlessedBLE library to facilitate communication with Enactsense. Namely, we used this library to search for and connect to Enactsense, to inform Enactsense of any modifications made to the scan parameters, to receive scan measurements from Enactsense, and to send instructions to Enactsense in order to remotely control the sample heater or electromagnet. The voltammetric scan parameters can either be manually entered by the user or imported by scanning custom QR codes, which we have designed to contain embedded information associated with a specific electrochemical biosensor. Editable parameters include the scan type, beginning potential, end potential, step potential, among other scan type specific parameters. We created several graphical animations to help walk the user through the various stages of a typical electrochemical experiment. These stages include connecting the on-chip electrodes to Enactsense, adding the sample to the on-chip electrodes, heating the sample, and performing the scan. Preloaded video demonstrations provide the user with additional guidance. We employed the MPAndroidChart open-source graphing

library to generate graphical representations of scan measurement (voltammograms). However, the raw data can also be saved locally on the device in comma-separated values (CSV) format.

Another key responsibility of the Android application is to perform signal processing. Owing to the noise background of electrochemical measurements that can at times be significant, data can be obfuscated leading to analytical errors[107]. To address this, various signal processing techniques have been proposed to smooth electrochemical datasets including moving median filters and Savitzky-Golay filters[108]. While moving median filters can be employed to help smooth the data, this approach can lead to truncated signal peaks[108]. Conversely, Savitzky-Golay filters more accurately preserve the structural integrity of the original signal[108–110]. As such, we employed Marcin Rzeźnicki's open-source SGFilter Java class to perform this data smoothening. It should be noted that this approach does not address the fact that baseline currents, resulting from the composition of the WE, electrolyte, presence of dissolved oxygen, and experimental ambient conditions, can obscure the true peak amplitude of a signal[111]. In order to remove the above-mentioned baseline currents, we developed a moving average baseline correction algorithm. This algorithm computes the moving average baseline and subtracts this curve from the raw signal. The last analytical function we developed for the smartphone application is a simple peak detection algorithm that returns a list of local maxima and minima.

From a firmware perspective, we employ two external libraries: the ArduinoBLE library which is used to facilitate BLE communication, and Sparkfun's ADS122C04 Arduino library which is used to interface with the ADC and properly configure its registers. A function was developed to automatically reconfigure the sampling rate of the ADC based on the timing parameters of the voltammetric scan, allowing for improved signal-to-noise ratios when performing slower voltammetric scans. Individual functions were created for each of the

supported voltammetric scan types. Timer interrupts are used to appropriately update the DAC output and poll from the ADC in accordance with the scan's timing parameters. In order to support biosensing experiments with dual signal electrodes, the firmware toggles the MAX4644EUT so that sequential electrochemical measurements can be performed.

Electrical and Electrochemical Characterization

The noise performance, as well as the electrochemical performance of Enactsense, were investigated and compared to the commercially available Sensit Smart, a widely-used miniaturized potentiostat by PalmSens. Electrochemical biosensing experiments are susceptible to electrical noise given their low signal amplitude and/or high frequency[107]. This unwanted distortion of the output signal can be generated intrinsically through the electrical components of the potentiostat or coupled from an external source. Open circuit noise measurements were performed to quantify the input-referred noise of Enactsense. It was found that the standard deviation of the open-circuit noise was greater than the effective resolution of the ADC (36 pA *versus* 19 pA). As such, the current sensing abilities of Enactsense are limited by the input-referred noise of the device rather than the resolution of the ADC itself.

To understand the electrochemical performance of Enactsense, we performed cyclic voltammetry using the $[Fe(CN)_6]^{4-}$/ $[Fe(CN)_6]^{3-}$ redox couple at five different concentrations (2 mM, 1 mM, 0.5 mM, 0.25 mM, and 0 mM) with a scan rate of 200 mV/s. Based on this scan rate, the ADC sampling rate for Enactsense was automatically set to 600 SPS. The performance of Enactsense was compared to the commercially-available Sensit Smart. The resulting voltammograms as recorded by Enactsense and Sensit Smart can be found in Figure 3.2A and Figure 3.2C respectively. A more detailed breakdown can be found in SI Table 3.3.

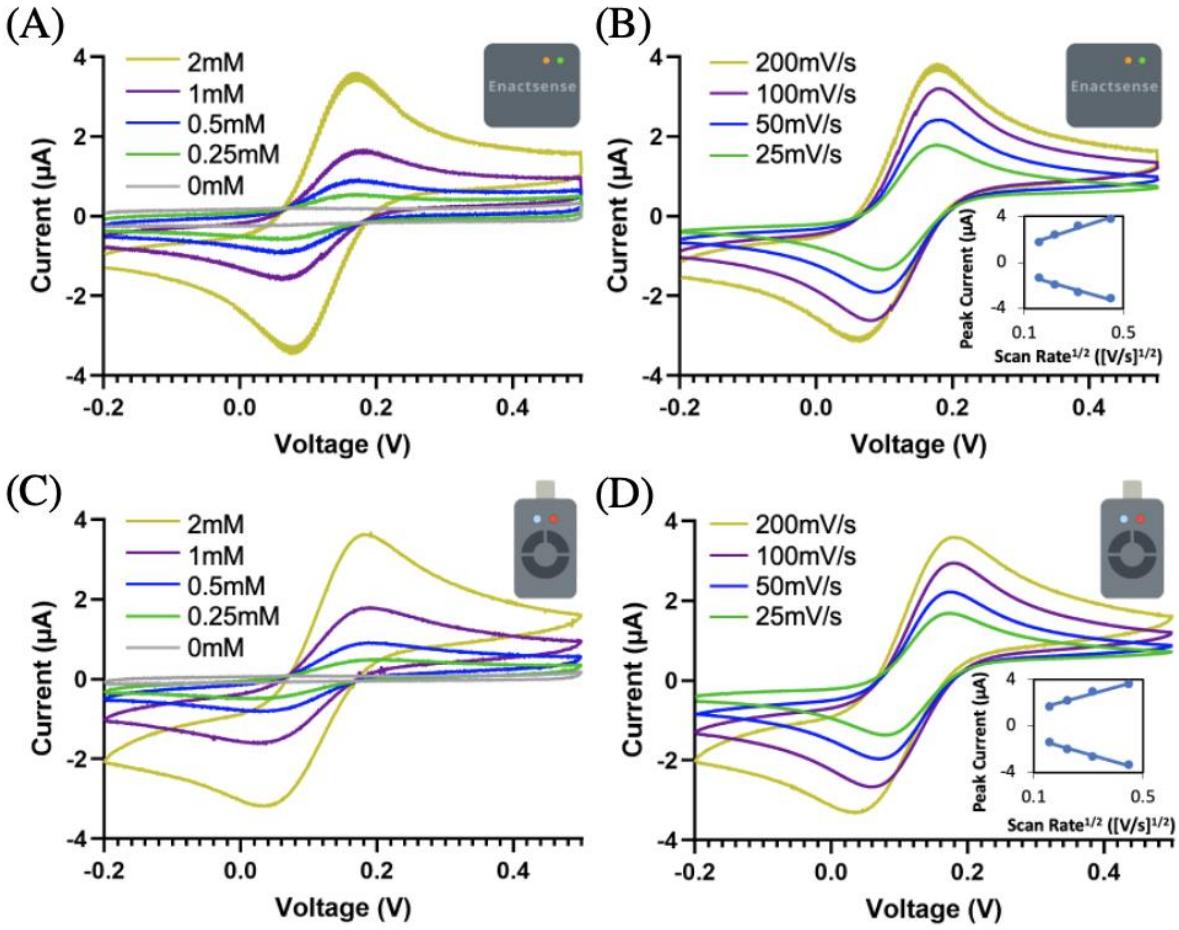

Figure 3.2: Comparison of cyclic voltammetry measurements between Enactsense and a commercial device. (A) Cyclic voltammogram of different concentrations of a $[Fe(CN)_6]^{4-}$/ $[Fe(CN)_6]^{3-}$ recorded using Enactsense and on-chip electrodes with a scan rate of 200mV/s. (B) Cyclic voltammogram of 2mM $[Fe(CN)_6]^{4-}$/ $[Fe(CN)_6]^{3-}$ recorded using Enactsense and on-chip electrode at variable scan rates. The inset highlights the linear relationship that was observed between the peak current and the square root of the scan rate. (C) Cyclic voltammogram of different concentrations of $[Fe(CN)_6]^{4-}$/ $[Fe(CN)_6]^{3-}$ recorded using a commercial potentiostat and on-chip electrodes with a scan rate of 200mV/s (D) Cyclic voltammogram of 2mM $[Fe(CN)_6]^{4-}$/ $[Fe(CN)_6]^{3-}$ recorded using a commercial potentiostat and on-chip electrode at variable scan rates. The inset highlights the linear relationship that was observed between the peak current and the square root of the scan rate.

Using a concentration of 2 mM of $[Fe(CN)_6]^{4-}$/ $[Fe(CN)_6]^{3-}$, cyclic voltammetry was performed at four different scan rates (200 mV/s, 100 mV/s, 50 mV/s, and 25 mV/s). This corresponds to sampling rates of 600 SPS, 175 SPS, 90 SPS, and 45 SPS, which were automatically determined by the firmware (Appendix 3.3). The resulting voltammograms as

recorded by Enactsense and Sensit Smart can be found in Figure 3.2B and Figure 3.2D respectively. The cyclic voltammograms show a linear change in peak current with respect to the square root of scan rate (Inset- Figure 3.2C-D) demonstrating the expected diffusion-controlled behaviour[112]. A more detailed breakdown can be found in SI Table 3.4.

The peak currents and voltages and peak shapes as recorded by Enactsense, and the commercial device are similar. Differences can partly be attributed to variation between the individual on-chip electrodes. It should be noted; however, that the noise performance of Enactsense improved when lower ADC sampling rates were used, hence why the high scan rate datasets appear noisier in comparison to the commercial device. Given the black-box nature of the commercial device, it is unknown if any signal filtration or processing is automatically conducted post-data collection. Data smoothening was not applied to Enactsense datasets.

Peripheral Devices Validation

Solution heating is used in a broad range of biosensing experiments for sample preparation (*e.g.* lysis) and/or for expediting binding kinetics (*e.g.* DNA hybridization)[16]. To enable the translation of electrochemical biosensors with such requirements from the laboratory to the market, a portable heater, operated by Enactsense, was created (Figure 3.3A). To demonstrate the effectiveness of this sample heater, an on-chip electrode was heated, targeting 37°C, for 30 minutes. It was found that the surface temperature of the on-chip electrode reached 37°C after approximately 15 minutes and plateaued at roughly 40°C after 20 minutes (Figure 3.3B). Future iterations of the sample heater should pre-heat the on-chip electrode in order to combat the long heating ramp time. We further evaluated the sample heater peripheral by using it in a DNA hybridization experiment (Figure 3.3C). In this experiment, single-stranded probe DNA was immobilized on the surface of the working electrode. The target DNA sequence was

tagged with methylene blue, a redox reporter. The hybridization of the immobilized probe with the redox DNA results in the generation of a signal. To detect DNA hybridization, square wave voltammetry was performed before and after target incubation. As previously discussed, data processing (Savitzky-Golay filtering and baseline subtraction) was conducted in-app. It was found that the heated on-chip electrodes incubated with target DNA produced a detectible signal with an average value of 20.5nA, whereas those that were incubated at room temperature did not (Figure 3.3D). The reproducible nature of these results demonstrate the effectiveness of the sample heater in promoting suitable conditions for DNA hybridization.

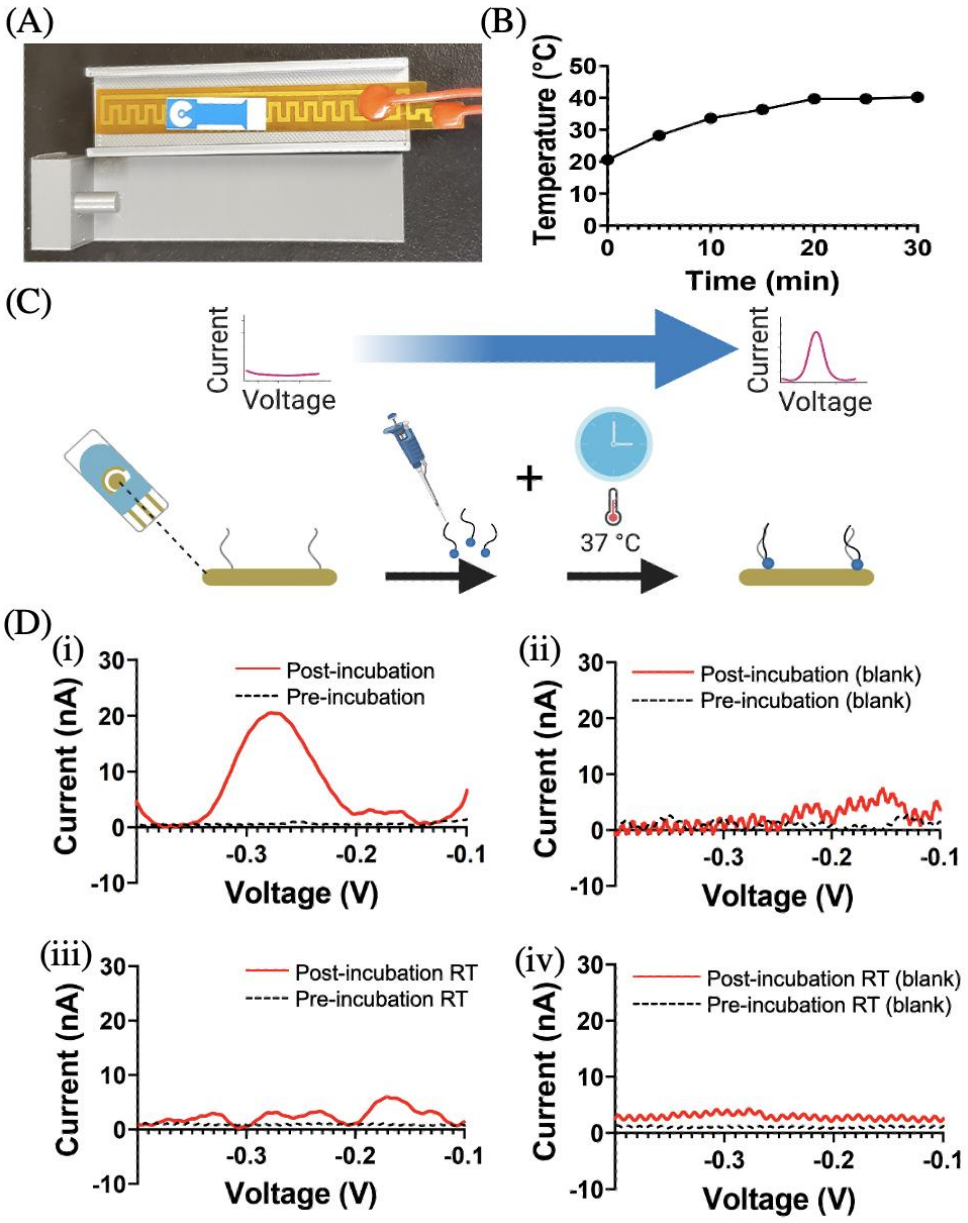

Figure 3.3: Sample heater validation. (A) A top-down view of the sample heater peripheral device. (B) Recorded surface temperature of the on-chip electrodes in the sample heater as a function of time. (C) Working principles of the bio-barcode assay. Probe DNA is deposited onto the surface of the WE. After depositing redox DNA, the on-chip electrodes are left to incubate for 30 minutes at 37°C to facilitate hybridization with the probe. (D) Representative square wave voltammograms of the bio-barcode assay recorded using Enactsense with on-chip electrodes before and after depositing: (i) 150nM of target DNA and incubating for 30 minutes at approximately 37°C using the portable sample heater peripheral; (ii) 150 nM of target DNA and incubating for 30 minutes at room temperature; (iii) blank target and incubating for 30 minutes at approximately 37°C using the portable sample heater peripheral; (iv) blank target and incubating for 30 minutes at room temperature.

In order to showcase Enactsense's magnetic manipulation capabilities, it was used to isolate magnetic microbeads in solution. The electromagnet was turned on and placed directly beside a rectangular vial filled with a solution of 14µL of DI water and 1µL of magnetic microbeads as shown in Figure 3.4A for 30 minutes. We adopted this specific orientation in order to highlight that the formation of the magnetic microbead congregation was not the result of gravitational forces. As shown in Figure 3.4B and Figure 3.4C respectively, photographs of the vial were taken before and after this experiment to showcase the formation of the magnetic microbead congregation. Further research must be conducted to confirm the viability of this peripheral device for use with electrochemical assays.

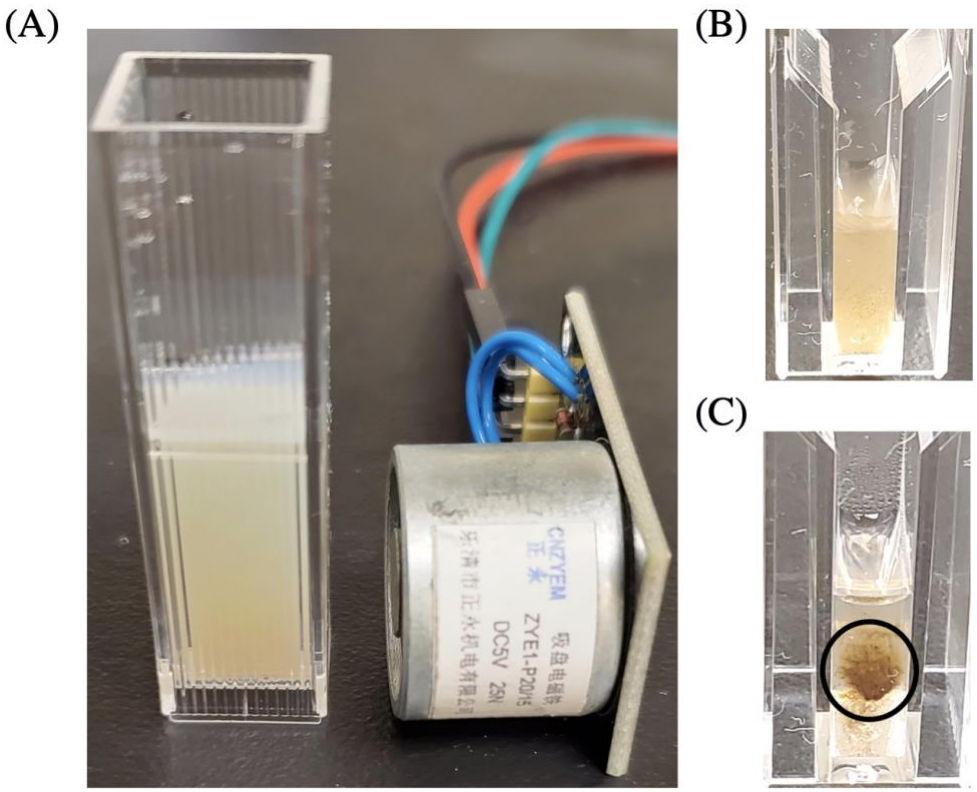

Figure 3.4: Electromagnet validation. (A) Photograph of the experimental setup. Photographs of a vial containing a mixture of DI water and magnetic beads before (B) and after (C) running the electromagnet for 30 minutes.

Evaluation of a Two-Working Electrode Assay

Multiplexing is used in biological assays to evaluate a single sample for multiple target analytes and/or to obtain multiple readings per analyte for improved assay reliability[43,113–116]. For such assays, it is necessary for the potentiostat to read out signals generated on multiple electrodes. To demonstrate Enactsense's compatibility with multiplexed assays, we used it in conjunction with a two-working electrode assay[43]. Briefly, this assay uses two working electrodes to detect *E. coli*. *E. coli* specific RNA-cleaving DNAzyme probes that are designed to cleave a segment of themselves in the presence of the target are surface-immobilized on the first electrode[43,117]. Single-stranded DNA probes, which are designed to capture the cleaved segment of the DNAzyme, are surface-immobilized on the second electrode. In the presence of *E. coli*, the assay is designed to show a signal decrease on the first electrode and a signal increase on the second electrode.

To validate the applicability of Enactsense with the above-mentioned two-working electrode assay, square wave voltammograms were recorded at each stage of the assay operation (Figure 3.5B), using the MAX4644EUT to automatically toggle between the two electrodes. As expected, in the presence of *E. coli*, the peak current decreased on the first electrode and increased on the second electrode. For the blank solution, the signal still decreased on the first electrode, likely due to DNAzyme degradation[118]; however, the signal changed by a much lesser amount on the second electrode in comparison to the target solution. The signal change on the two electrodes was calculated by subtracting the pre-target peak current from the post-target peak current and dividing the result by the pre-target peak current. In the event that no clear peaks were observed, as was the case with two of the first electrodes with target, the RMS noise values were used in place of the peak current. Data smoothening was not performed in these cases. On the first electrode, signal changes of 0.52 and 0.31 were observed for the target and

blank samples, respectively, demonstrating a measurable difference (signal-to-blank ratio of 1.68) between the two samples. On the second electrode, much higher signal changes were measured using the target (84) and blank (6) samples, resulting in a remarkable signal-to-blank ratio of 14. Given the large signal changes on the second electrode, the data obtained from this electrode is more suitable for bioanalytical sensing. Nevertheless, the data obtained from the first electrode is critical for validating the quality of the manufactured chips.

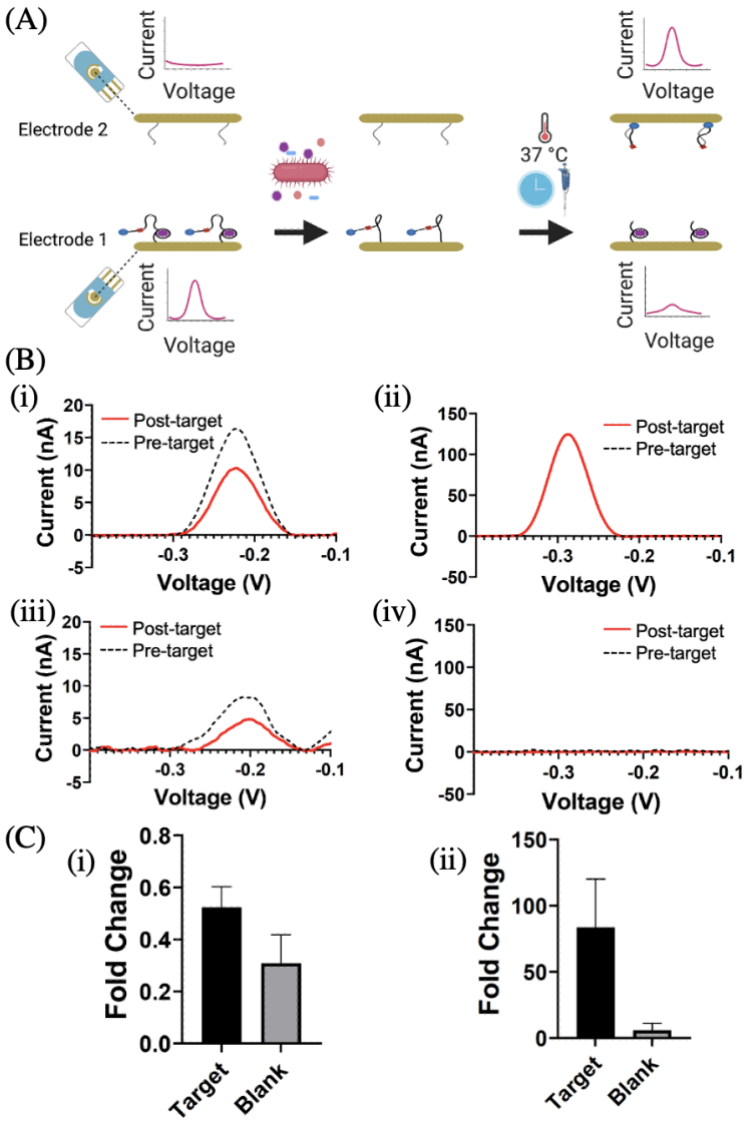

Figure 3.5: Evaluation of Enactsense for multiplexed analysis (A) Schematic illustration of the two-electrode assay. In the pre-target phase, the first electrode shows a large redox signal due to the redox tag on the DNAzyme, whereas the second electrode does not exhibit a signal. Following target incubation on Electrode 1, the DNAzymes are cleaved, and the redox DNA barcode, causing a decrease in the measured electrochemical current. The solution is then manually pipetted onto the second electrode. Following the incubation of the solution on the second electrode, the DNA barcode binding results in a large redox signal. (B) Square wave voltammetry as recorded using Enactsense. (i) Electrode 1 measurements pre- and post-incubation with 10^6 CFU/mL intracellular mixture of E. coli. (ii) Electrode 2 measurements pre- and post-incubation with the solution transferred from Electrode 1. (iii) Electrode 1 measurements pre- and post-incubation with a blank sample. (iv) Electrode 2 measurements pre- and post-incubation with a blank sample. (C) Fold changes for target and blank samples on (i) Electrode 1 and (ii) Electrode 2, target representing 10^6 CFU/mL intracellular mixture of E. coli. and black representing PMT20.

3.5 Conclusion

This work describes the design and validation of a smartphone-operated portable electrochemical reader and actuator (Enactsense) that is specifically designed for use with biological assays with heating, magnetic actuation, and multiplexed readout. Enactsense is wirelessly controlled by an accompanying smartphone via Bluetooth Low Energy technology. This device supports multiple voltammetric scan types, the parameters of which can be manually edited or imported automatically by scanning a QR code through the smartphone application. The collected scan data is transmitted from Enactsense to the smartphone for data smoothening, peak detection, and baseline correction. Electrochemical validation of Enactsense with $[Fe(CN)_6]^{4-}$/ $[Fe(CN)_6]^{3-}$ solutions yielded markedly similar results with a high-end commercially available portable potentiostat, wherein both devices recorded similar peak currents and produced similarly shaped curves . Unlike the commercial system, Enactsense features native multiplexing and actuating capabilities, which are designed to allow the rapid translation of biological assays from the laboratory to the market. Enactsense was also used for the detection of bacteria using a two-electrode assay, demonstrating the feasibility of using this system with complex, real-world assays. Future development of Enactsense could lead to the incorporation of machine learning classification algorithms and additional peripheral instruments.

3.6 Appendix

Appendix 3.1: Voltammetric Techniques

Individual functions were developed for each of the supported voltammetric techniques. Timer interrupts, of which the specific timing intervals are determined in accordance with the scan's timing parameters, are used such that the output to the DAC can be appropriately updated. Provided in Figure S3.1 is a composite of sample excitation waveforms for each of the supported voltammetric scan types as recorded using a Digilent Analog Discovery USB oscilloscope. Note, a 1.5V offset is applied to the excitation signals given that the Arduino Nano 33 BLE can only output values between 0V-3.3V. This offset is accounted for by a applying a 1.5V bias to the non-inverting terminals of both the control amplifier and transimpedance amplifier. To minimize input referred noise associated with the ADC, the minimum possible sampling rate is used based on the timing characteristics of the voltammetric scan. For square wave voltammetry, this is dependent on the frequency. For all other supported voltammetric techniques, the minimum ADC sampling rate is determined based on the scan rate.

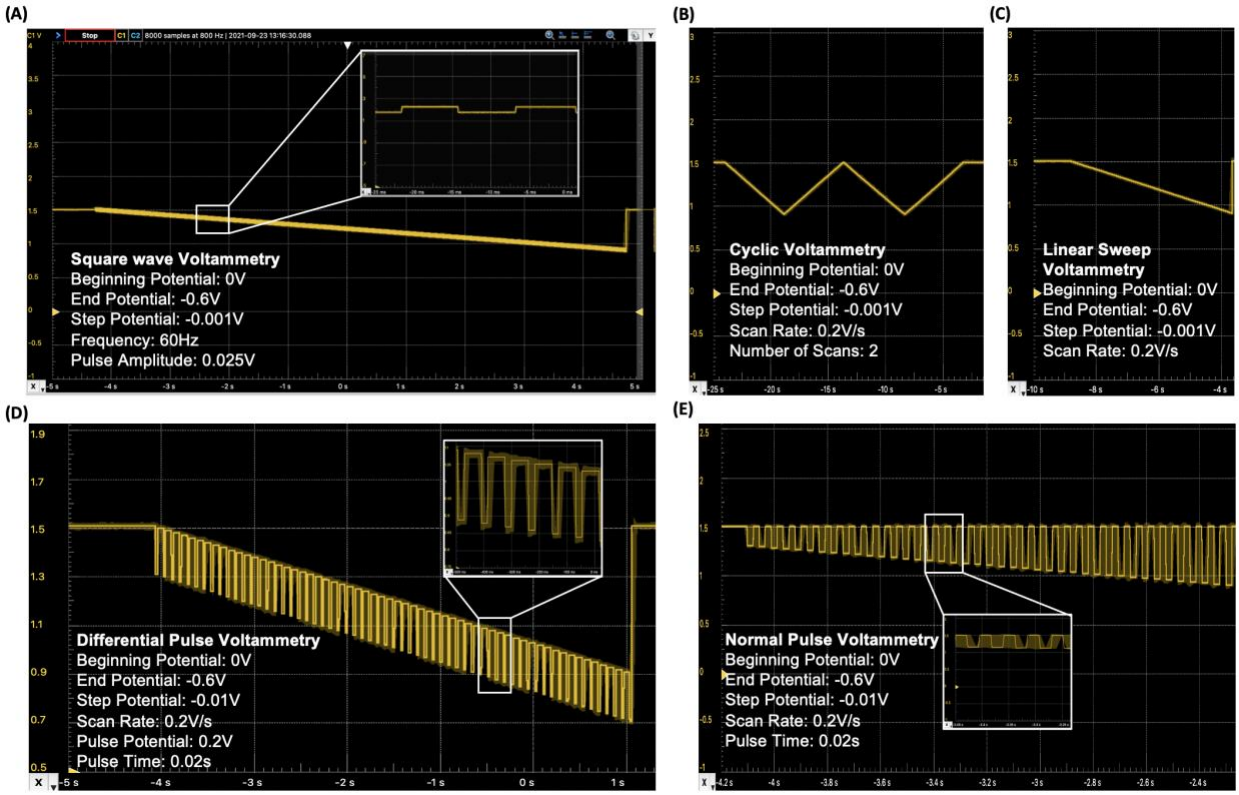

Figure S3.1: Sample voltammetric excitation waveforms. (A) Square wave voltammetry. (B) Cyclic voltammetry. (C) Linear sweep voltammetry. (D) Differential pulse voltammetry. (E) Normal Pulse Voltammetry.

Appendix 3.2: Supporting Tables

SI Table 3.1: DNA Sequences

TP (20 nt)	3′-Thiol	TAGCTAGGAAGAGTCACACA	Capture DNA probe
TD 79 nt	5′- Methylene blue; R = riboA; 3′-Thiol	MBTTTTTTGTGTGACTCTTCCTAGCT RTGGTTCGATCAAGAGATGTGCGTC TTGATCGAGACCTGCGACCGTTTTTT TTTTSH	*E.coli* DNAzyme

SI Table 3.2: Device Specifications

Supported Voltametric Scan types	Square wave voltammetry, cyclic voltammetry, linear sweep, differential pulse, normal pulse
Current range	-10µA to 10µA (-20µA to 20µA for differential methods)
Supply voltage	4.5-21V
Signal generation resolution	16-bit
Measurement resolution	24-bit (20-bit effective)
Measurement sampling rate	Programmable from 20sps – 2ksps
Output range	-1.5V to 1.5V

SI Table 3.3: Electrochemical Validation Comparison at Different Concentrations

Potentiostat	**Peak Cathodic Current (µA)**	**Difference in Peak Cathodic Current (E-reader – Sensit Smart)**	**Peak Anodic Current (µA)**	**Difference in Peak Anodic Current (E-reader – Sensit Smart)**
E-reader	0.33226 (0 mM) 0.546346 (0.25 mM) 0.910075 (0.5 mM) 1.64917 (1 mM) 3.576164 (2 mM)	0.15221 (0 mM) 0.053997 (0.25 mM) -0.00377 (0.5 mM) -0.14422 (1 mM) -0.074316 (2 mM)	-0.268641 (0 mM) -0.585902(0.25 mM) -0.922914 (0.5 mM) -1.584334 (1 mM) -3.435929 (2 mM)	-0.140619 (0 mM) 0.304144 (0.25 mM) 0.143536 (0.5 mM) 0.024606 (1 mM) -0.257239 (2 mM)
Sensit Smart	0.180039 (0 mM) 0.492349 (0.25 mM) 0.913845 (0.5 mM) 1.79339 (1 mM) 3.65048 (2 mM)		-0.127791 (0 mM) -0.890046 (0.25 mM) -1.06645 (0.5 mM) -1.60894 (1 mM) -3.17869 (2 mM)	

SI Table 3.4: Electrochemical Validation Comparison at Different Scan Rates

Potentiostat	**Peak Cathodic Current (µA)**	**Difference (E-reader – Sensit Smart)**	**Peak Anodic Current (µA)**	**Difference (E-reader – Sensit Smart)**
E-reader	1.780262 (25mV/s) 2.416615 (50mV/s) 3.200974 (100mV/s) 3.800662 (200mV/s)	0.095452 (25mV/s) 0.196745 (50mV/s) 0.256614 (100mV/s) 0.208282 (200mV/s)	-1.342545 (25mV/s) -1.912291 (50mV/s) - -2.618165 (100mV/s) -3.130803 (200mV/s)	0.023985 (25mV/s) 0.050329 (50mV/s) 0.047515(100mV/s) 0.185087 (200mV/s)
Sensit Smart	1.68481 (25mV/s) 2.21987 (50mV/s) 2.94436 (100mV/s) 3.59238 (200mV/s)		-1.36653 (25mV/s) -1.96262 (50mV/s) -- -2.66568 (100mV/s) -3.31589 (200mV/s)	

Appendix 3.3: ADC Sampling Rate Algorithm

Given that the noise performance of Enactsense is dependent on the ADC sampling rate, algorithms were developed to determine the minimum ADC sampling rate in accordance with the timing parameters of the voltammetric scan. In cyclic voltammetry, current is sampled after each step potential is applied. Accordingly, the cyclic voltammetry sampling rate is dependent on the scan rate and the step potential size as shown in Equation 3.1. In the case of square wave voltammetry, current must be sampled at the end of the return and forward pulse. As such, the square wave sampling rate is twice that of the frequency as shown Equation 3.2.

(3.1)

$$CV\ Sampling\ Rate = \frac{Scan\ Rate\ (Vs^{-1})}{Step\ potential\ (V)}$$

(3.2)

$$SWV\ Sampling\ Rate = Frequency\ (Hz) * 2$$

The minimum ADC sampling rate had to exceed the above scan-specific sampling rates. This minimum ADC sampling rate also had to account for the DAC and ADC conversion times. The DAC conversion time was experimentally determined by updating the output of the DAC for 5 minutes and measuring the difference in time pre and post conversion. The maximum recorded conversion time was found to be 1282µs. A similar procedure was followed to determine the ADC conversion times. Conversion times of 1371µs, 2039µs, 3400µs, 6125µs, 11600µs, 22563µs, and 50251µs were recorded for 1000SPS, 600SPS, 330SPS, 175SPS, 90SPS, 45SPS, and 20SPS respectively. As such, the minimum ADC sampling rate had to satisfy the condition shown in Equation 3.3, which includes a 100µs safety tolerance.

(3.3)

$$ADC\ Conversion\ Time > (Scan\ Specific\ Sampling\ Rate)^{-1} - DAC\ Conversion\ Time - 100\mu s$$

It should be noted that by minimizing the ADC sampling rate, noise may be under-sampled resulting in aliasing[106].

Chapter 4: A Portable and Smartphone-Operated Photoelectrochemical Reader for Point-of-Care Biosensing

4.1 Preface

The purpose of this chapter is to demonstrate the design and validation of a portable PEC reader featuring synchronous control of an optical excitation source. The challenges associated with adapting PEC for PoC use are discussed. The design of the PEC reader is outlined. Experiments were conducted to validate and demonstrate the versatility of this device.

Multiple authors have contributed to this chapter as it has recently been prepared for publication with the working title of "A Portable and Smartphone-Operated Photoelectrochemical Reader for Point-of-Care Biosensing" in Elctrochimica Acta. Sadman Sakib was responsible for preparing the biosensors. Alexander Scott was responsible for designing and programming the PEC reader. Both Alexander Scott and Sadman Sakib performed the PEC experiments and contributed to writing. Dr. Sudip Saha contributed to editing. In addition, Dr. Leyla Soleymani contributed to the design and writing of this section.

4.2 Introduction

Biosensors are devices that bring together biorecognition and signal transduction elements for analyzing biologically-relevant analytes[119–122]. These devices are ideally suited for use in point-of-care (PoC) diagnostics and health monitoring systems and are being extensively researched for diagnosing infectious diseases[43,123], cancers[2,3,124–126], cardiovascular diseases[126,127], and neurological diseases[125,128], to name a few. The rapid sample-to-result time of these devices at the point-of-need facilitates prompt and effective intervention by clinicians, which is expected to increase patient survivability and minimize the rates of disease transmission[20,129].

Multiple signal transduction strategies – electrochemical[20,43], photoelectrochemical[122,130–132], electronic[133,134], optical[135,136], and mechanical[134,137] – have been widely used in biosensing[138].

Among these, photoelectrochemical (PEC) signal transduction, combining optical excitation with electrochemical readout, has generated tremendous interest due to its low limit-of-detection (LOD)[139], high sensitivity[26], and broad linear dynamic range[140]. The decoupling of the mode of signal excitation from the signal readout reduces the background signals that are generated at high voltage biases, enhancing the signal-to-background ratio and limit-of-detection of PEC biosensors[11,26,27,122,141].

The increasing number of PEC biosensors reported in the literature (from 35 search results up to 2011 on Pubmed to an additional 764 results up to 2021), is in stark contrast to the lack of such biosensors available in commercial markets. In many cases, this can be attributed to the limited number of suitable photoactive materials that meet the stringent chemical stability requirement of biosensors and the challenges resulting from the poor photostability of common reagents and analytes (e.g. DNA probes, antibodies, antigens) under high energy excitation[11,122,142]. Such issues are being addressed by researchers through the development of new chemically-stable photoactive materials such as semiconductor metal oxides[11,132,143,144], quantum dots[145–147], and carbon-based nanomaterials[148–150] and the use of photocurrent enhancing strategies such as creating hybrid plasmonic nanoparticle-metal oxide nanostructures[151,152], using carbon nanomaterials as highly conductive scaffolds[153,154], using organic ligands/dyes to improve optical absorption[131,155], and dual sensitization via coupling large & small bandgap semiconductors[156,157] for exciting these materials at lower energies (i.e. visible wavelengths). The limited commercial success of PEC biosensors is further compounded by the challenges associated with employing existing PEC readout devices for PoC use. While PEC workstations are commercially available, they are both prohibitively expensive and are not portable in nature. These devices are also feature rich, consisting of frequency analyzers, potentiostats, photodiode sensors, and tunable light

sources. However, many of these features are of no use in a PoC capacity. Conversely, none of the commercially available portable potentiostats[13,14] support PEC biosensing, and their functionality cannot be expanded given their black-box nature[71]. In the same vein, none of the lab-made potentiostats reported in the literature[9,68,70,72,78,158] can interface with or control optical-excitation sources and accordingly do not support PEC biosensing. Despite the promising potential of PEC biosensors as a PoC diagnostic technique, the need for a portable PEC readout device has gone unnoticed by both researchers and industry alike.

As such, we sought to develop a portable and low-cost smartphone-operated PEC readout system to help expedite the translation of PEC biosensors from the laboratory to the real world. In particular, this device, referred to hereon as PECsense, can perform voltammetric measurements while synchronously controlling an optical-excitation source. This solution is made possible due to the increased processing power and decreasing cost of both smartphones and microcontrollers alongside both the widespread global adoption of smartphones in recent years and the development of low-energy consumption communication protocols like Bluetooth Low Energy (BLE). Cathodic/anodic currents were measured in response to different biases, and both rapid PEC cycling tests and long-term optical exposure tests were conducted in order to demonstrate the versatility and robustness of PECsense. The performance of PECsense was further compared to a commercial PEC readout device. Finally, to demonstrate the applicability of this newly-developed PEC reader, we used it alongside TiO_2 photoelectrodes for PEC DNA biosensing. In order to distinguish between matched and mismatched DNA, we used PECsense to measure the change in photocurrent before and after DNA capture.

4.3. Materials and Methods

Materials and photoelectrode fabrication

Caffeic acid (CA) and 100 nm indium tin oxide coated poly(ethylene terephthalate) (ITO/PET) were purchased from Sigma-Aldrich. TiO_2 nanoparticles (P25, containing 80% anatase and 20% rutile) were obtained from Nippon Aerosil Co. Ltd. An aqueous suspension of 0.66 g/L TiO_2 nanoparticles was prepared, to which a solution of CA dissolved in 5% ethanol solution was added to produce CA-surface modified TiO_2 nanoparticles (CA-TiO2). The mass ratio of TiO_2 to CA in the CA-TiO_2 suspension was 10:1. ITO/PET substrates with dimensions of 1.2 cm × 0.7 cm were masked with vinyl to preserve the electrical contact area. Substrates were subjected to (oxygen) plasma treatment for 1 min. The substrates were then coated with CA-TiO_2 by depositing 10μL of the suspension on the substrate surface and incubating in the oven at 85°C for 6 min. This process was repeated three times to deposit three layers.

Device Design

PECsense was tailored around the sensing parameters of the TiO_2 nanoparticle surface modified with CA (CA-TiO_2) biosensor previously developed by Sakib et al[132]. In order to perform PEC biosensing, PECsense can perform voltammetric techniques while synchronously controlling an LED matrix circuit which is used as an optical excitation source. This LED matrix circuit consists of four QT-Brightek PLCC6 white LEDs that have a neutral white color temperature (typically 4240K) and a typical intensity of 6000mcd. Printed circuit boards (PCB) for PECsense and the LED matrix circuit were designed using Eagle Autodesk and manufactured by JLCPCB. The electronic components were then hand-soldered onto the PCBs. The firmware was created using the Arduino integrated development environment and the accompanying Android application was written in Java using the Android Studio integrated development environment.

Device Characterization

A standard three-electrode cell setup was used with white light as a photoexcitation source. A platinum (Pt) wire was used as the counter electrode, a silver/silver chloride (Ag/AgCl) electrode for the reference electrode and the CA-TiO_2 photoelectrodes served as the working electrodes. The custom-made LED matrix circuit was used as an optical excitation source. The electrolyte solution used for the biasing experiment was composed of 0.5 M sodium hydroxide (NaOH) solution, whereas the electrolyte solution used for both the rapid PEC cycling and long-term exposure experiments was composed of 0.1 M phosphate-buffered solution (PBS) and 0.1 M ascorbic acid (AA). The photocurrent measurement was done by running PECsense in chronoamperometric mode. The potential of the photoelectrode was fixed at 0 V, except for in the biasing experiment where the potential was varied. The performance of PECsense was compared to the Zahner CIMPS-QE/IPCE PEC workstation.

DNA Hybridization and Detection Experiments

DNA detection testing was conducted using CA-TiO2 photoelectrodes, a PBS/AA electrolyte solution, and the LED matrix circuit as a photoexcitation source. When measuring the photocurrent of the PEC cell, the potential was kept constant at 0 V and the working electrode was irradiated for 40 s in the middle of a 120 s runtime. A solution of 20 mM 1-ethyl-3-(3-dimethylaminopropyl)carbodiimide hydrochloride (EDC), 10 mM N-hydroxysulfosuccinimide (NHS), and 10 mM 2-(N-morpholino)ethanesulfonic acid (MES) was deposited onto the photoelectrodes and incubated for 1 hour. This was done in order to facilitate carboxamide linking between CA and amine-terminated probe single-stranded DNA (ssDNA). Subsequently, 1 μM amine-terminated probe DNA was deposited on the photoelectrode surface and incubated for 2.5 hours. The photocurrent was measured at this point to get the after-probe photocurrent.

This was followed by the deposition of 100 nM target ssDNA, which was incubated for 1 hour. To test non-specific adsorption, some samples were spiked with 100 nM non-complementary ssDNA and/or 10% human blood plasma. The photoelectrodes were washed between each deposition step with DI water. The photocurrent was once again measured at this point to get after-target photocurrents. All the photocurrents were normalized by adjusting the after-probe photocurrents to the same level and multiplying the after-target photocurrent with the same adjustment factor. The photocurrents were further normalized by performing baseline subtraction.

4.4 Results

Device Design

We have developed a portable (75 mm by 40 mm, <100g including a 3D printed case) and inexpensive (~100 USD) PEC reader, referred to as PECsense, which is wirelessly controlled by an Android application through the Bluetooth Low Energy (BLE) communication protocol to facilitate away-from-lab PEC experiments. In this design, we capitalize on the widespread global adoption of BLE-supported smartphones, rendering our system both smaller and less expensive than a standalone device. The specifications of PECsense are summarized in Table 4.1.

Table 4.1: PECsense specifications

Supported scan types	Square wave voltammetry, cyclic voltammetry, linear sweep, differential pulse, normal pulse, chronoamperometry
Current range	-10μA to 10μA (-20μA to 20μA for differential measurements)
Supply voltage	4.5-21V
Signal generation resolution	16-bit (46μV quantization error)
ADC resolution	24-bit
Experimental current sensing resolution	36pA
Sampling rate	Programmable from 20sps – 1000sps (20sps used in this work)
Typical LED matrix color temperature	4240K
Typical LED matrix intensity	6000mcd

Alongside standard components that commonly make up a potentiostat (Figure 4.1A) – a core processing unit (Arduino Nano 33 BLE development board), a digital-to-analog converter (DAC), a reconstruction filter, potentiostat circuitry consisting of a voltage follower (VF), control amplifier (CAmp), and transimpedance amplifier (TIA), and an analog-to-digital converter (ADC) – our device also interfaces with a peripheral LED matrix circuit (Figure 4.1B) for PEC signal readout. The independence of the LED matrix circuit from the core device allows it to be modified to meet the optical requirements of different PEC assays. In this case, white LEDs were used as it had previously been demonstrated that the surface modified TiO_2 photoelectrodes were photoactive in the near-UV region and the visible part of the spectra[132].

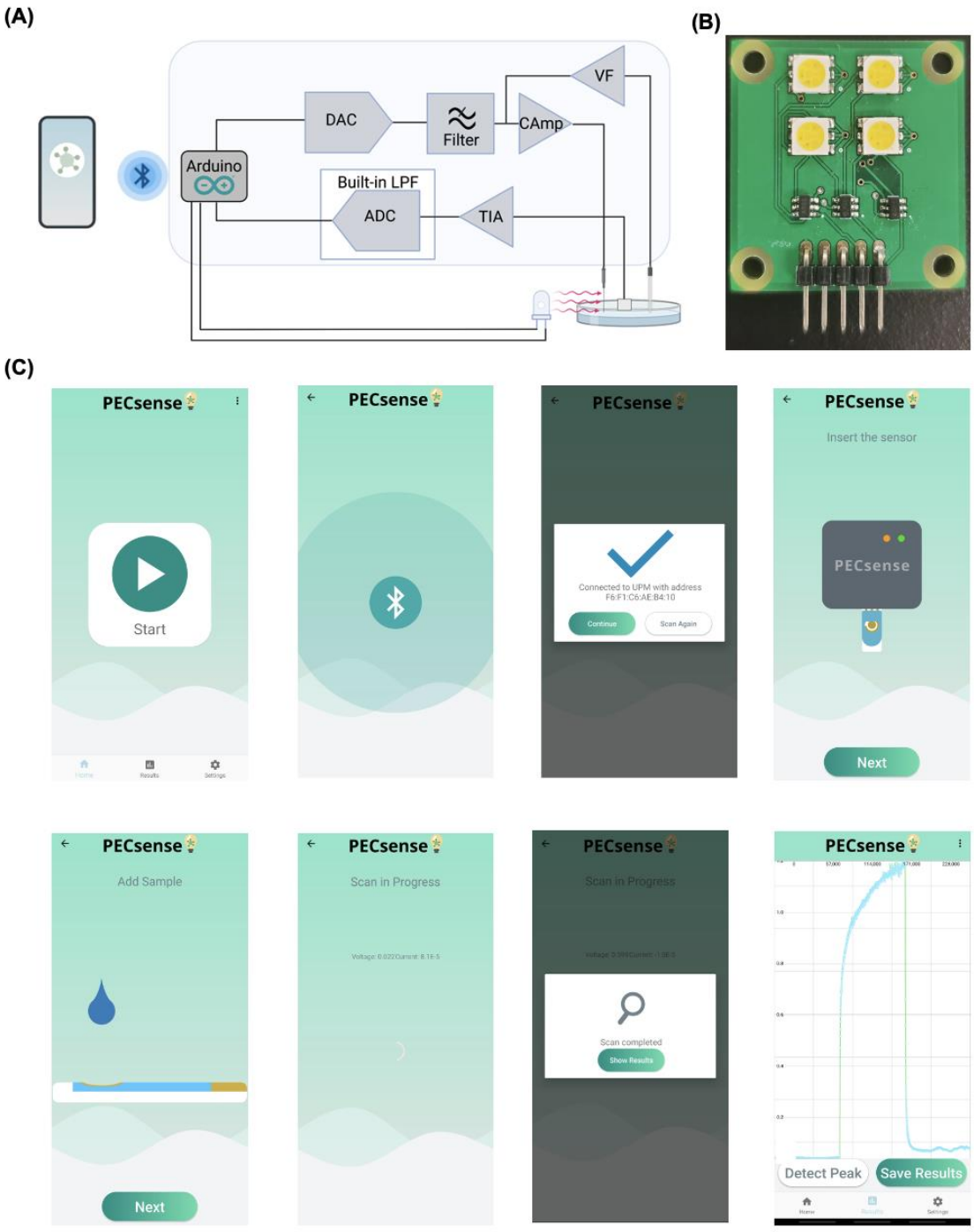

Figure 4.1: Overview of PECsense. (A) A block diagram representation of PECsense consisting of the Arduino Nano 33 BLE development board, digital-to-analog converter (DAC), reconstruction filter, core-potentiostat circuit composed of a voltage follower (VF), control amplifier (CAmp), and transimpedance amplifier (TIA), and analog-to-digital converter (ADC) with a built-in low-pass filter (LPF). (B) Photograph of the LED matrix circuit. (C) The smartphone application process flow.

We developed a firmware function to perform chronoamperometric scans while synchronously controlling the LED matrix circuit. This function makes use of timer interrupts to toggle the LED matrix circuit ON and OFF. Scan parameters including the LED on and off time, the total duration of the scan, the voltage bias, pulse amplitude, pulse duration, and the sampling rate are all adjusted using the accompanying smartphone application. We undertook significant effort when designing the smartphone application to ensure it could easily be controlled even by inexperienced users. By providing graphical animations, the Android application guides the user through the different stages of a typical PEC experiment (Figure 4.1C). The collected scan measurements are then transmitted from PECsense to the smartphone via BLE for signal processing and to compile the results in a graphical format. In particular, we have developed functions to perform in-app peak detection and data smoothening using a Savitzky-Golay filter, an algorithm known for smoothening while preserving the shape and key features of the original signal[108–110].

Device Characterization

Experiments were conducted to demonstrate the versatility of PECsense and highlight its applicability for a wide array of PEC experiments. In order to demonstrate PECsense's ability to measure anodic and cathodic photocurrents, we applied different bias voltages (-1.0V, -0.75V, 0.75V, 1.0V) in conjunction with an NaOH electrolyte solution and measured the resulting photocurrent. It was expected that the positive biases would yield anodic currents, and the negative biases would generate cathodic currents due to the oxidation of water and reduction of oxygen species, respectively. The working photoelectrodes, constructed via the drop deposition of TiO_2 nanoparticle suspensions onto a conductive polymer substrate, were irradiated with white light using the LED matrix circuit at 30 s intervals for 150 s, in order to generate the

chronoamperometric curves (Figure 4.2). As expected, the results demonstrated that PECsense could measure cathodic and anodic currents when positive and negative biases were applied. However, in the case of both the -0.75V and 0.75V biases, the signals were obfuscated by noise given their low amplitude. The noise can partly be attributed to the lack of shielding from background illumination and electrical interference. It is well known that the cathodic photocurrent generation of metal oxides in alkaline solutions saturate in the region of -0.9 V to -1.0 V[159]. This saturation is attributed to the diffusion limitation of oxygen species, thus limiting the reduction reaction[159]. This explains the large increase in cathodic photocurrent from -0.75 V bias to -1.0 V bias, as the system has not yet reached saturation. In contrast, the anodic photocurrent generation experiences saturation at a lower bias level of around 0.5 V. Accordingly, the anodic photocurrent increase from 0.75 V to 1.0 V is much lower[159].

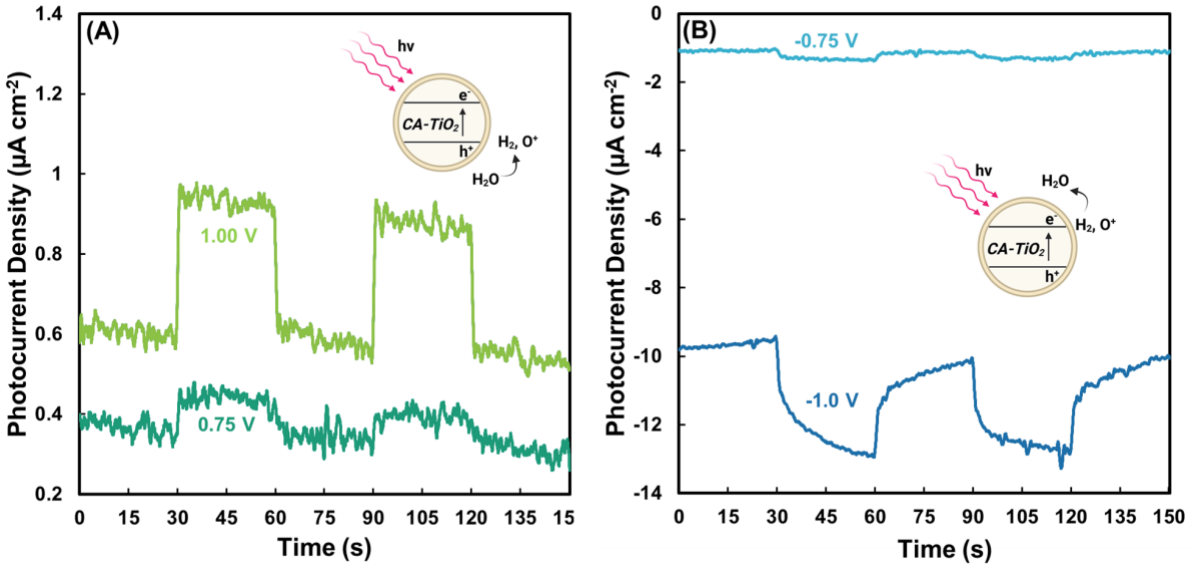

Figure 4.2: Applied bias experiments using the PEC reader. (A) Anodic photocurrent generated by CA-TiO_2 photoelectrodes at bias voltages of 0.75 V and 1.0 V using this device. The inset illustrates photocurrent generation via oxidation of water. (B) Cathodic photocurrent generated by CA-TiO_2 photoelectrodes at bias voltages of -0.75 V and -1.0 V using this device. The inset illustrates photocurrent generation via reduction of oxygen species.

To further demonstrate the robustness of PECsense and showcase its applicability for PEC measurements with variable illumination periods, we conducted a PEC cycling test. The potential of the photoelectrode was held constant at 0 V bias and concurrently irradiated with white light using the LED matrix circuit at 20-s intervals for 20 minutes (Figure 4.3A). This experiment was replicated using the same LED matrix circuit and the Zahner CIMPS-QE/IPCE PEC workstation, a benchtop measurement system used as a control (Figure 4.3B). The two systems resulted in similar PEC currents that followed the illumination pattern, with gradual ramping of the photocurrents observed during the first 15 cycles. This behavior is owed to the photo-charging effect where charge carriers are built-up at the photoelectrode/electrolyte and substrate/photoelectrode interfaces, producing a capacitive charging response[160,161]. The short light-ON periods are not enough to reach the steady-state of the capacitive response, and some discharge occurs at a slower rate during the light-OFF periods, resulting in the sawtooth photocurrent waveforms. The small decreases in photocurrent observed near the latter half of the experiment can be attributed to mechanical degradation of the photoelectrodes due to rapid cycling. Differences in the results obtained from PECsense and Zahner CIMPS-QE/IPCE PEC workstation can largely be attributed to variability between photoelectrodes and the fact that the Zahner CIMPS-QE/IPCE PEC workstation was better shielded from background illumination and interference through the use of a faraday cage. This faraday cage was not used in conjunction with PECsense in order to better replicate the typical conditions associated with PoC measurements. This likely explains the larger photocurrent density observed using PECsense when the LED matrix circuit was toggled OFF. To investigate the electrical performance of PECsense, the input-referred noise was characterized. This parameter is a measure of the electrical noise due to the circuit barring any interference induced by the PEC cell. The working

electrode connector was left open and readings were taken for 7 minutes. The ADC sampling rate was set to 20 sample-per-second, thereby enabling the built-in 50/60 Hz low-pass filter. This sampling rate is in line with all other measurements conducted in this work. The standard deviation of the open-circuit noise measurement was found to be 36 pA. While no direct comparison is publicly available, preliminary results for the Zahner CIMPS-QE/IPCE PEC workstation indicate that the current accuracy is 0.01% of full scale for measurements in the 1 µA – 100 mA and 0.1% of full scale outside of that range[162].

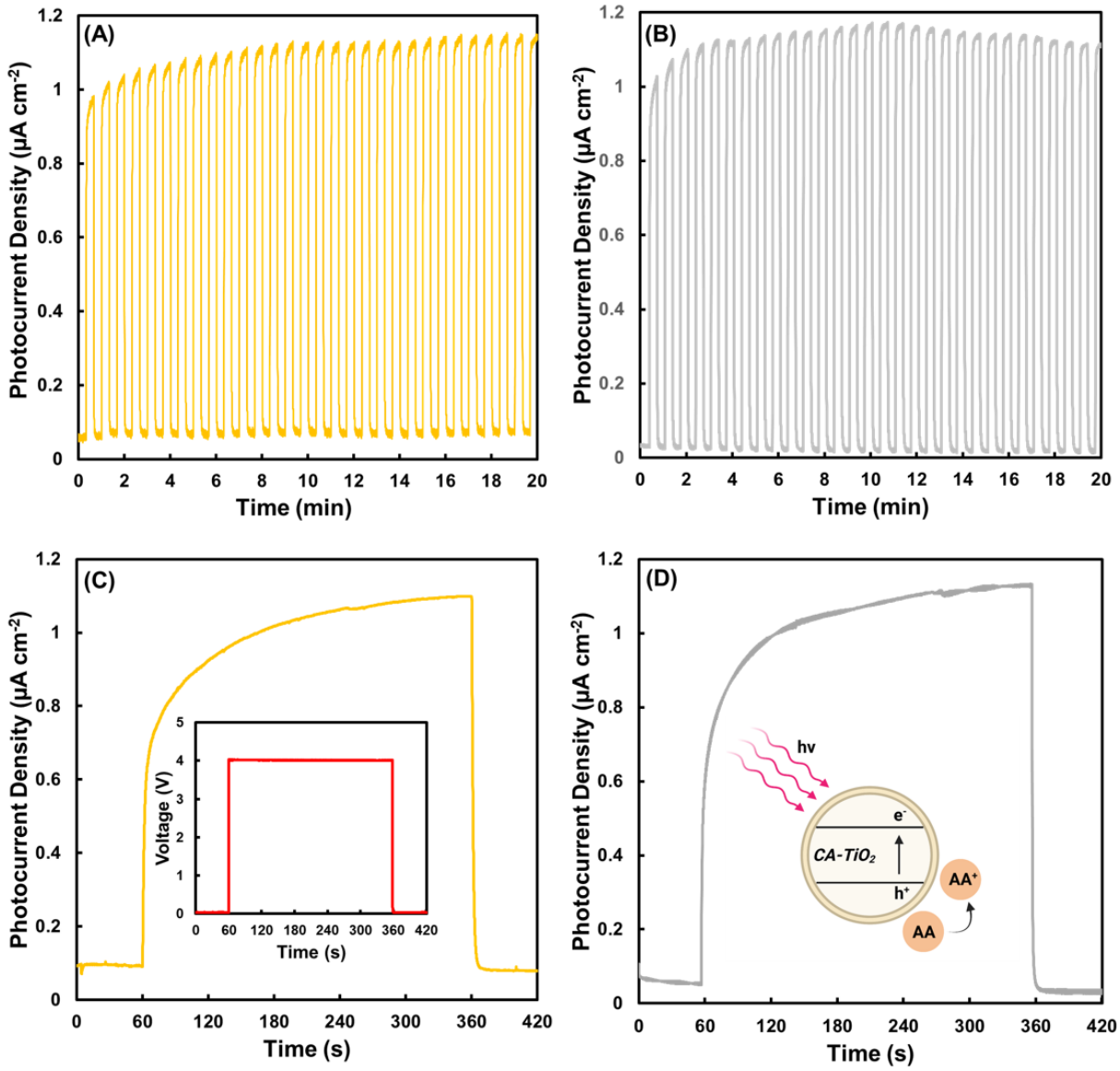

Figure 4.3: Variable illumination experiments conducted using PECsense and a commercial PEC workstation. (A) PEC cycling test conducted using PECsense. (B) PEC cycling test conducted using the Zahner CIMPS-QE/IPCE PEC workstation. (C) Long term exposure test conducted using PECsense. Inset shows LED matrix intensity measurement using a photocell. (D) Long term exposure test using the Zahner CIMPS-QE/IPCE PEC workstation. Inset illustrates photocurrent generation via the oxidation of ascorbic acid following TiO_2 photoexcitation.

Next, we performed a long-term exposure test in order to demonstrate that the LED matrix circuit could be used as a stable optical excitation source without significant fluctuations. Photocurrent measurements were conducted using a PBS/AA electrolyte solution. The AA electrolyte is a hole scavenger and its oxidation at the photoelectrode results in the generation of anodic photocurrent (Figure 4.3D inset). The potential of the PEC cell was held constant at a 0V bias, and the working photoelectrode was irradiated with white light using the LED matrix circuit for 5 minutes, in order to generate the chronoamperometric curve (Figure 4.3C). The performance was compared to the Zahner CIMPS-QE/IPCE PEC workstation (Figure 4.3D). As shown in Figure 4.3, an anodic current is generated due to the oxidation of ascorbic acid at the working electrode when under illumination. Additionally, the PEC curves measured using PECsense are nearly indistinguishable from those recorded by the Zahner CIMPS-QE/IPCE PEC workstation, featuring similar shapes and peak photocurrents. Using a photocell, we measured the luminosity of the LED matrix circuit over a 5-minute period (Figure 4.3C inset) to verify consistent performance of the LED matrix circuit. Throughout this 5-minute period, the resistance of the photocell remained constant, indicating that the luminosity of the LED matrix circuit was stable. The photo-charging effect observed for the PEC cycling test is also present in the long-term exposure test. However, without the intermittent discharging, the photocurrent was able to come close to achieving steady-state within the 5-minute LED matrix circuit ON period.

DNA Hybridization and Detection Experiments

In order to demonstrate the applicability of our newly developed handheld platform for PEC biosensing, we used it to detect signal changes in a DNA hybridization detection assay[132]. To this end, we fabricated photoelectrodes through drop deposition of TiO_2 nanoparticle suspensions onto a conductive polymer substrate. Briefly, the main mechanism for detection of

this signal-OFF type biosensor is based on the photocurrent decrease due to steric hindrance following deposition of probe, which limits the access of electrolyte species with the photoelectrode surface and the capture of target ssDNA through DNA hybridization[122,132,163,164] (Figure 4.4A and 4.4B).

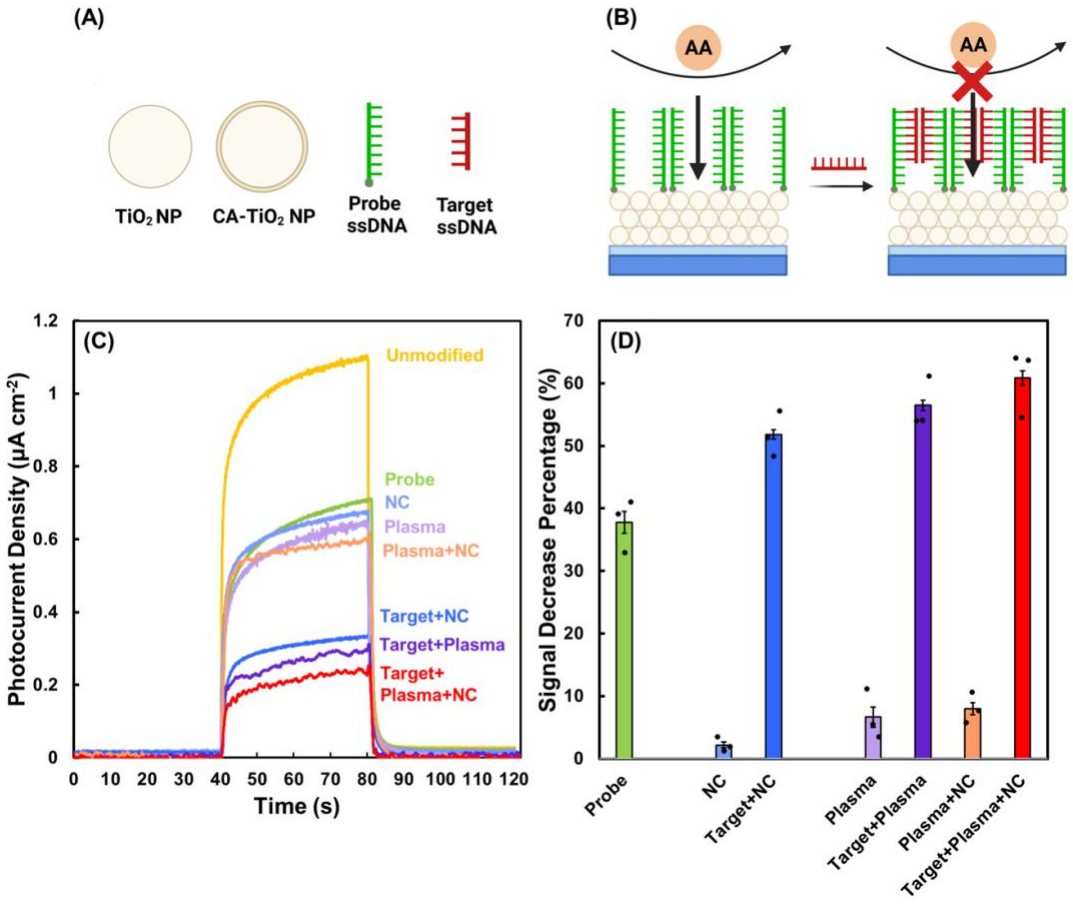

Figure 4.4: DNA biosensor operation and data collection using PECsense. (A) Unmodified TiO_2, CA-modified TiO_2, probe DNA and target DNA. (B) DNA detection scheme. Following hybridization with target DNA, photocurrent decreases due to steric hinderance in the presence of ascorbic acid. (C) Photocurrent densities at unmodified, after-probe and after-target stages of signal-OFF DNA biosensor operation. The after-target samples include: only non-complementary target in buffer (NC), non-complementary target & complementary target in buffer (Target+NC), only human blood plasma (Plasma), complementary target in human blood plasma (Target+Plasma), non-complementary target in human blood plasma (Plasma+NC), and both non-complementary target & complementary target in human blood plasma. (D) Summary of photocurrent signal decrease at each stage of the signal-OFF DNA biosensor operation.

To validate the performance of PECsense, we measured the photocurrent density after each stage of the operational process: unmodified; after-probe deposition; and after-target stages (Figure 4.4C). Using this data, we calculated the percent reduction in photocurrent relative to the previous stage (Figure 4.4D). The unmodified photoelectrodes were composed of TiO_2 nanoparticles that were surface modified with caffeic acid to improve photocurrent generation through photo-absorption enhancement[131,132,141]. The peak photocurrent density of the unmodified stage was found to be 1.12 μA cm^{-2}. The deposition of 1 μM probe ssDNA resulted in a 37.7 % average signal decrease. In the after-target stage, deposition of 100 nM non-complementary ssDNA in buffer (NC) as a control resulted in a slight 2.1 % decrease in signal, which can attributed to non-specific DNA adsorption on the photoelectrode[27,165]. In comparison, when a solution of 100 nM non-complementary and 100nM complementary target ssDNA in buffer (Target+NC) was deposited, the observed signal reduction was much larger at 51.8 %, due to DNA hybridization[27,122]. The four other samples in the after-target stage all contained 10% human blood plasma and showed a slightly higher signal decrease compared to the samples in buffer. This is due to higher non-specific absorption, and the presence of additional proteins and biomolecules in human blood plasma[166]. The control samples containing only plasma (Plasma) and those containing 100nM non-complementary ssDNA spiked in plasma (Plasma+NC) showed a signal decrease of 6.6 % and 8.0 %, respectively. The sample with 100nM target complementary ssDNA in plasma (Target+Plasma) displayed a 56.5 % signal reduction, whereas the sample with both 100nM non-complementary ssDNA and 100nM target complementary ssDNA spiked in plasma (Target+Plasma+NC) showed a higher signal reduction at 60.9 %. While the protocol as presented in this work is slightly modified, these results are in-line with those previously reported by Sakib et al.[132], which were recorded using a commercial PEC

workstation. Accordingly, this demonstrates that the sensing abilities of PECsense is suitable for PEC DNA biosensing

4.5 Conclusion

A portable PEC reader (PECsense) has been validated using TiO_2 surface-modified PEC DNA biosensors. Unlike other potentiostats reported in the literature[9,68,70,72,78,158] and even many commercial systems[13,14], this device interfaces with a custom LED matrix circuit to facilitate PEC experiments. It was found that PECsense offered similar levels of performance to the commercially available Zahner CIMPS-QE/IPCE PEC workstation at a fraction of the cost and in a significantly smaller form factor. We demonstrated that PECsense could be used in a number of different PEC applications, including experiments with variable illumination periods, those that yield cathodic and anodic currents, and those that operate under different potential biases. The independent nature of the LED matrix circuit from the core PEC readout device means that modifications can easily be made to the LED matrix to suit a specific PEC experiment. It is our hope that the device presented in this work can help transition PEC biosensing away from being conducted exclusively within a laboratory setting.

Chapter 5: Conclusion

5.1 Thesis Summary

In Chapter 1, we highlighted the growing need for PoC diagnostic devices and introduced electrochemical and PEC biosensing, two sensing modalities that show significant promise for PoC use. Some of the key challenges associated with adapting these sensing modalities for PoC use were discussed and the motivations and objectives for this work were presented.

The aim of Chapter 2 was to provide the reader with the necessary background to understand this work by providing brief reviews on the following topics:

1. Electrochemical and PEC biosensing;
2. DNA and DNAzyme based biosensors; and,
3. Operating principles and development trends of potentiostats.

In Chapter 3, a portable smartphone-operated electrochemical reader was developed and evaluated. The hardware design was detailed and an overview of the firmware and accompanying smartphone application was presented. This chapter consists of three sets of experiments, the key findings of which are as follows.

1. Electrical and electrochemical characterization: The noise characteristics of the reader were determined through open-circuit noise analysis. The standard deviation of the input-referred noise was found to be 36pA. This value is greater than the resolution offered by the ADC, indicating that the current sensing resolution is noise-limited. The electrochemical performance of this device was compared to the commercially available Sensit Smart. Cyclic voltammetry of $[Fe(CN)_6]^{4-}$/ $[Fe(CN)_6]^{3-}$ at various scan rates and concentrations were conducted. Despite the significantly lower cost of the reader

developed herein, the cyclic voltammograms of the two systems exhibited similar peak anodic and cathodic currents and peak voltages.

2. Peripheral device validation: A portable sample heater consisting of a flexible adhesive polyimide resistive heating element that could be controlled directly by the electrochemical reader was designed. This heater was used to promote DNA hybridization in a DNA bio-barcode three-electrode assay. A commercially available electromagnet module was also integrated and controlled by the electrochemical reader to isolate magnetic microbeads in a vial.
3. Differential signal multiplexed assay: The electrochemical reader was used to perform sequential measurements of a dual signal assay for ultralow detection of *E.coli*. without the need for any manual reconfiguration of the electrodes. This assay consists of two working electrodes. The first contains surface-immobilized RNA-cleaving DNAzymes which release methylene blue tagged DNA in the presence of target DNA, resulting in a signal decrease. The second working electrode contains surface-immobilized DNA bio-barcodes that selectively hybridize with the aforementioned methylene blue tagged DNA, leading to the generation of a signal. In the presence of target DNA, the first electrode experienced a notable signal decrease with an average fold change of 0.52. Likewise, the average fold change for the second electrode was found to be 84. Conversely, for those on-chip electrodes that were incubated with a blank solution, electrode 1 and electrode 2 exhibited an average fold change of 0.31 and 6 respectively. Unlike other potentiostats, our electrochemical reader does not require any manual reconfiguration or hardware add-ons to support sequential measurement of dual signal multiplexed assays.

In Chapter 4, the readout system that was presented in Chapter 3 was adapted for PEC biosensing. The modifications to the hardware, firmware, and software needed to support this new sensing modality were discussed. This chapter consists of two sets of experiments, a summary of the key findings can be found below.

1. Device versatility: To demonstrate the effectiveness of the PEC reader as a robust PEC biosensing platform, several experiments were conducted. First, PEC cells with an NaOH electrolyte were held at different biases in order to demonstrate the PEC reader's ability to record both cathodic and anodic photocurrent. PEC cycling tests were conducted with the PEC reader and the commercially available Zahner CIMPS-QE/IPCE PEC workstation whereby the working electrode was irradiated with white light at 20-s intervals for 20 minutes. It was found that the two devices yielded markedly similar peak photocurrent densities and PEC curve shapes. Long-term exposure tests were also conducted wherein the working electrode was irradiated with white light for 5 minutes. Again, our PEC reader yielded very similar results to the Zahner CIMPS-QE/IPCE PEC workstation producing similar shapes and peak photocurrent densities. Using a photocell, the luminosity of the optical excitation source peripheral luminosity was confirmed to be stable over the 5-minute period.
2. PEC DNA biosensing: Photoelectrodes made of TiO_2 NP surface modified with caffeic acid were constructed. The PEC reader was used to synchronously control an optical excitation source and measure the resulting photocurrent. Photocurrent density was measured using the PEC reader after fabrication, post probe deposition, and following incubation with target. Relative to unmodified photoelectrodes, the percent reduction in photocurrent density following probe deposition was 37.7%. 100nM non-complimentary

ssDNA reduced the photocurrent density by 2.1% relative to the after-probe photocurrent density. On the other hand, 100nM non-complimentary plus 100nM complimentary DNA yielded a 51.8% reduction in photocurrent density. It was found that samples with human blood plasma yielded slightly larger photocurrent density reductions likely resulting from the addition of proteins and higher non-specific absorption. These results were in-line with those previously recorded using Zahner CIMPS-QE/IPCE PEC workstation, indicating that our PEC reader meets the stringent requirements for PEC DNA biosensing.

5.2 Contributions to the Field

This work contributes to the advancement of the field in five key areas.

1. *Low cost, portable, high-performance potentiostat*

While there continues to be a need for sophisticated and highly accurate potentiostats by researchers, the high cost associated with these devices can limit the implementation of electrochemical and PEC biosensors in a PoC capacity. Conversely, our device is a low-cost and portable alternative that offers high performance, comparable to some commercially available options.

2. *Away-from-lab sample preparation and signal actuation*

While several other low-cost potentiostats have been reported in the literature, none to our knowledge have attempted to integrate auxiliary instruments like heating units and electromagnets despite their use in a number of different electrochemical and PEC contexts. These instruments are often large and laboratory-bound, inherently preventing any

electrochemical or PEC biosensors with such requirements from being used outside of a laboratory setting. In this work, a proof-of-concept heater peripheral was designed that can be controlled automatically by the reader. This heater was used to perform the sample heating requirements associated with a DNA bio-barcode assay. Similarly, an electromagnet was used to perform magnetic manipulation. Following this approach, additional peripheral devices can be designed that will expand upon the actuating abilities of the reader and facilitate the adoption of biosensors with such auxiliary device dependencies outside of laboratory settings.

3. Point-of-care photoelectrochemical biosensing

To our knowledge, there has yet to be a laboratory-made potentiostat capable of supporting PEC biosensing. As such, our reader was designed to interface with and synchronously control a peripheral LED matrix circuit consisting of four QT-Brightek PLCC6 white LEDs expands. Our reader possesses many of the same adjustable parameters as a commercially available PEC workstation, thereby enabling our reader to be used in a number of different PEC applications. This includes experiments with variable illumination periods, potential biases, and experiments that yield cathodic or anodic photocurrents.

4. Native compatibility with dual signal electrodes

Unlike commercial systems and other low-cost potentiostats reported in the literature, our reader does not require any external hardware add-ons to support dual signal assays with two working electrodes. Our reader was designed to support these assays out-of-the-box and makes use of the MAX4644EUT switch to toggle between two working electrodes in order to perform sequential measurements. This is important as in many cases, the detection of multiple disease biomarkers may be required for an accurate diagnosis.

5. PoC user centric software

Our accompanying smartphone application has been tailored for PoC users that may be unfamiliar with the electrochemical/photoelectrochemical process. This is in contrast to most laboratory-made potentiostats which provide little more user interface than adjustable scan parameters, start buttons, and voltammograms. Graphical illustrations are provided to help guide the user through the typical stages of electrochemical and photoelectrochemical experiments. In addition, an innovative system was developed to circumvent the manual configuration of scan parameters whereby these parameters can be imported automatically by scanning in an assay-specific QR code. Video files are preloaded in the application to provide further guidance to the user. The smartphone application can also perform key data processing functions, including data smoothening, baseline subtraction, and peak detection.

5.3 Future Work

Future iterations of the reader should expand upon the device's capabilities in four key areas. This will allow future iterations of the readout system to better meet the previously outlined design goals.

1. Design and validate additional peripheral devices

   In this work, a peripheral sample heater, electromagnet, and an LED matrix were validated. Additional peripheral devices, such as microfluidic pumping systems, could be incorporated to further expand the sensing capabilities of our reader. This will expedite the transition of complex biosensors outside of laboratory settings towards PoC applications.
2. Electrochemical Impedance Spectroscopy

At present, our reader only supports voltammetric techniques. The ADC possesses a maximum sampling rate of 2kSPS which is insufficient for many EIS experiments. In order to support EIS, an ADC with a higher sampling rate or a dedicated impedance converter system (such as the AD5933 from Analog Devices) can be used instead. The AD5933 is I2C compatible and features an onboard frequency generator and DSP engine. This engine can be used to compute the real and imaginary components at each frequency, so that the EIS magnitude and phase can easily be determined. Such hardware modifications will allow our readout system to support even more biosensors.

3. Augmented analytical capabilities supported by machine learning.

   Machine learning algorithms can be incorporated to improve the analytical capabilities of our reader in a number of different ways. For example, support vector machine can be used to classify the presence or absence of a target analyte. Machine learning algorithms can also be employed for biofouling detection, noise reduction, and classification in multiplexed systems. An ever-expanding suite of machine learning tools can be used to facilitate model training and deployment on the accompanying Android application. The development of such algorithms will render our readout system more approachable as users will no longer be required to manually decipher scan results.

4. Device optimization

   Our readout system and its associated peripheral devices can be optimized in several ways. Ensuring the device was easy to hand-solder was the primary concern when designing the PCB layout. Accordingly, little consideration was taken to minimize cross-talk and electromagnetic interference. These factors should be considered when developing future iterations. Similarly, the device footprint could be minimized. In

conjunction, a proper housing unit could be developed with electromagnetic shielding abilities to further minimize the impact of electromagnetic interference. To facilitate firmware development, we based our readout system around the Arduino Nano 33 BLE board. However, this board includes a number of features that went unused including a built-in 12-bit ADC and inertial measurement unit. As such, future iterations of this reader could replace the Arduino Nano 33 BLE board with a lower cost BLE-supported microcontroller. The peripheral devices described in this work are proof of concepts, and several modifications can be made to their form factor to improve their overall performance.

References

(1) US Department of Health and Human Services; CDC. Antibiotic Resistance Threats in the United States. *Centers Dis. Control Prev.* **2019**, 1–113.

(2) Traynor, S. M.; Pandey, R.; Maclachlan, R.; Hosseini, A.; Didar, T. F.; Li, F.; Soleymani, L. Review—Recent Advances in Electrochemical Detection of Prostate Specific Antigen (PSA) in Clinically-Relevant Samples. *J. Electrochem. Soc.* **2020**, *167* (3), 037551. https://doi.org/10.1149/1945-7111/ab69fd.

(3) Bianchi, V.; Mattarozzi, M.; Giannetto, M.; Boni, A.; De Munari, I.; Careri, M. A Self-Calibrating Iot Portable Electrochemical Immunosensor for Serum Human Epididymis Protein 4 as a Tumor Biomarker for Ovarian Cancer. *Sensors (Switzerland)* **2020**, *20* (7). https://doi.org/10.3390/s20072016.

(4) Au/Australianprescriber, O. Full Text Free Online at Nps Non-Culture Methods for Detecting Infection. **2016**, *39* (5), 171–175.

(5) Lazcka, O.; Campo, F. J. Del; Muñoz, F. X. Pathogen Detection: A Perspective of Traditional Methods and Biosensors. *Biosens. Bioelectron.* **2007**, *22* (7), 1205–1217. https://doi.org/10.1016/j.bios.2006.06.036.

(6) Mahmood, T.; Yang, P. C. Western Blot: Technique, Theory, and Trouble Shooting. *N. Am. J. Med. Sci.* **2012**, *4* (9), 429–434. https://doi.org/10.4103/1947-2714.100998.

(7) Álvarez-Barrientos, A.; Arroyo, J.; Cantón, R.; Nombela, C.; Sánchez-Pérez, M. Applications of Flow Cytometry to Clinical Microbiology. *Clin. Microbiol. Rev.* **2000**, *13* (2), 167–195. https://doi.org/10.1128/CMR.13.2.167-195.2000.

(8) Fass, L. Imaging and Cancer: A Review. *Mol. Oncol.* **2008**, *2* (2), 115–152. https://doi.org/10.1016/j.molonc.2008.04.001.

(9) Sun, A. C.; Hall, D. A. Point-of-Care Smartphone-Based Electrochemical Biosensing. *Electroanalysis* **2019**, *31* (1), 2–16. https://doi.org/10.1002/elan.201800474.

(10) Liu, A.; Wang, K.; Weng, S.; Lei, Y.; Lin, L.; Chen, W.; Lin, X.; Chen, Y. Development of Electrochemical DNA Biosensors. *TrAC - Trends Anal. Chem.* **2012**, *37*, 101–111. https://doi.org/10.1016/j.trac.2012.03.008.

(11) Devadoss, A.; Sudhagar, P.; Terashima, C.; Nakata, K.; Fujishima, A. Photoelectrochemical Biosensors: New Insights into Promising Photoelectrodes and Signal Amplification Strategies. *J. Photochem. Photobiol. C Photochem. Rev.* **2015**, *24*, 43–63. https://doi.org/10.1016/j.jphotochemrev.2015.06.002.

(12) Grieshaber, D.; MacKenzie, R.; Vörös, J.; Reimhult, E. Electrochemical Biosensors - Sensor Principles and Architectures. *Sensors* **2008**, *8* (3), 1400–1458. https://doi.org/10.3390/s8031400.

(13) Palmsens. Palmsens 4 - Palmsens https://www.palmsens.com/product/palmsens4/ (accessed Sep 19, 2021).

(14) Palmsens. Sensit Smart - Palmsens.

(15) Impedance, G.; Eis, A. MStat-i 400 (Bi)Potentiostat/Galvanostat/Impedance Analyzer (EIS) MStat-i 400s Potentiostat/Galvanostat/Impedance Analyzer (EIS) 01. *400*.

(16) Billings, P. R. Three Barriers to Innovative Diagnostics. *Nat. Biotechnol.* **2006**, *24* (8), 917–918. https://doi.org/10.1038/nbt0806-917.

(17) Xu, Y.; Wang, E. Electrochemical Biosensors Based on Magnetic Micro/Nano Particles. *Electrochim. Acta* **2012**, *84*, 62–73. https://doi.org/10.1016/j.electacta.2012.03.147.

(18) Yamanaka, K.; Vestergaard, M. C.; Tamiya, E. Printable Electrochemical Biosensors: A Focus on Screen-Printed Electrodes and Their Application. *Sensors (Switzerland)* **2016**,

16 (10), 1–16. https://doi.org/10.3390/s16101761.
(19) Pumera, M.; Sanchez, S.; Ichinose, I.; Tang, J. Electrochemical Nanobiosensors. *Sensors Actuators B Chem.* **2007**, *123* (2), 1195–1205.
(20) Cesewski, E.; Johnson, B. N. Electrochemical Biosensors for Pathogen Detection. *Biosens. Bioelectron.* **2020**, *159* (April), 112214. https://doi.org/10.1016/j.bios.2020.112214.
(21) Hernández, H. H.; Reynoso, A. M. R.; González, J. C. T.; Morán, C. O. G.; Hernández, J. G. M.; Ruiz, A. M.; Cruz, J. M. H.; Orozco, R. Electrochemical Impedance Spectroscopy (EIS): A Review Study of Basic Aspects of the Corrosion Mechanism Applied to SteelsElectrochemical Impedance Spectroscopy (EIS): A Review Study of Basic Aspects of the Corrosion Mechanism Applied to Steels. *Intech* **2016**, *i* (tourism), 13.
(22) Randviir, E. P.; Banks, C. E. Electrochemical Impedance Spectroscopy: An Overview of Bioanalytical Applications. *Anal. Methods* **2013**, *5* (5), 1098–1115. https://doi.org/10.1039/c3ay26476a.
(23) Bard, A.; Faulkner, L.; Leddy, J.; Zoski, C. *Electrochemical Methods: Fundamentals and Applications*; 1980.
(24) Elgrishi, N.; Rountree, K. J.; McCarthy, B. D.; Rountree, E. S.; Eisenhart, T. T.; Dempsey, J. L. A Practical Beginner's Guide to Cyclic Voltammetry. *J. Chem. Educ.* **2018**, *95* (2), 197–206. https://doi.org/10.1021/acs.jchemed.7b00361.
(25) Kounaves, S. P. Voltammetric Techniques. In *Handbook of Instrumental Techniques for Analytical Chemistry*; Settle, F. A., Ed.; Prentice Hall PTR: Upper Saddle River, New Jersey, 1997; pp 711–720.
(26) Zhao, W. W.; Xu, J. J.; Chen, H. Y. Photoelectrochemical Immunoassays. *Anal. Chem.* **2018**, *90* (1), 615–627. https://doi.org/10.1021/acs.analchem.7b04672.
(27) Zhao, W. W.; Xu, J. J.; Chen, H. Y. Photoelectrochemical DNA Biosensors. *Chemical Reviews*. American Chemical Society August 13, 2014, pp 7421–7441. https://doi.org/10.1021/cr500100j.
(28) Westboek, P. Electrochemical Methods. In *Analytical Electrochemistry in Textiles*; Westbroek, P., Priniotakis, G., Kiekens, P., Eds.; Woodhead Publishing, 2005; pp 37–69. https://doi.org/https://doi.org/10.1533/9781845690878.1.37.
(29) Simões, F. R.; Xavier, M. G. Electrochemical Sensors. In *Nanoscience and its Applications*; Róz, A. L. Da, Ferreira, M., Leite, F. de L., Oliveira, O. N., Eds.; William Andrew Publishing: Cambridge, MA, United States, 2017; pp 155–178. https://doi.org/9780323497800.
(30) Nnamchi, P. S.; Obayi, C. S. Electrochemical Characterization of Nanomaterials. In *Characterization of Nanomaterials*; Bhagyaraj, S. M., Oluwafemi, O. S., Kalarikkal, N., Thomas, S., Eds.; Woodhead Publishing, 2018; pp 103–127. https://doi.org/https://doi.org/10.1016/B978-0-08-101973-3.00004-3.
(31) Bontempelli, G.; Dossi, N.; Toniolo, R. Voltammetry | Polarography. In *Encyclopedia of Analytical Science (Third Edition)*; Worsfold, P., Poole, C., Townshend, A., Miró, M., Eds.; Academic Press, 2019; pp 218–229. https://doi.org/https://doi.org/10.1016/B978-0-12-409547-2.14326-4.
(32) Franklin, R. K.; Martin, S. M.; Strong, T. D.; Brown, R. B. Chemical and Biological Systems: Chemical Sensing Systems for Liquids. In *Material Science and Material Engineering*; Franklin, R. K., Martin, S. M., Strong, T. D., Brown, R. B., Eds.; Elsevier, 2016. https://doi.org/https://doi.org/10.1016/B978-0-12-803581-8.00549-X.

(33) Mortimer, R. J. Spectroelectrochemistry, Methods and Instrumentation. In *Encyclopedia of Spectroscopy and Spectrometry*; Lindon, J. C., Tranter, G. E., Koppenaal, D. W., Eds.; Academic Press, 2017; pp 172–177. https://doi.org/https://doi.org/10.1016/B978-0-12-803224-4.00289-2.

(34) Morales, M. A.; Halpern, J. M. Guide to Selecting a Biorecognition Element for Biosensors. *Bioconjug. Chem.* **2018**, *29* (10), 3231–3239. https://doi.org/10.1021/acs.bioconjchem.8b00592.

(35) Sorochinskii, V. V.; Kurganov, B. I. Diffusion-Kinetic Theory of Stationary Behaviour of Amperometric Bienzyme Electrodes. *Biosens. Bioelectron.* **1996**, *11* (8), 709–718. https://doi.org/10.1016/0956-5663(96)85921-5.

(36) Sorochinskii, V. V; Kurganov, B. I. Amperometric Biosensors with a Laminated Distribution of Enzymes in Their Coating. Steady-State Kinetics. *Biosens. Bioelectron.* **1996**, *11* (1), 45–51. https://doi.org/10.1016/0956-5663(96)83712-2.

(37) Liu, D.; Perdue, R. K.; Sun, L.; Crooks, R. M. Immobilization of DNA onto Poly(Dimethylsiloxane) Surfaces and Application to a Microelectrochemical Enzyme-Amplified DNA Hybridization Assay. *Langmuir* **2004**, *20* (14), 5905–5910. https://doi.org/10.1021/la049605p.

(38) Díaz-Fernández, A.; Miranda-Castro, R.; de-los-Santos-Álvarez, N.; Rodríguez, E. F.; Lobo-Castañón, M. J. Focusing Aptamer Selection on the Glycan Structure of Prostate-Specific Antigen: Toward More Specific Detection of Prostate Cancer. *Biosens. Bioelectron.* **2019**, *128*, 83–90. https://doi.org/10.1016/J.BIOS.2018.12.040.

(39) Lu, Y.; Li, X.; Zhang, L.; Yu, P.; Su, L.; Mao, L. Aptamer-Based Electrochemical Sensors with Aptamer-Complementary DNA Oligonucleotides as Probe. **2008**. https://doi.org/10.1021/ac7018014.

(40) Yang, D.; Cheng, W.; Chen, X.; Tang, Y.; Miao, P. Ultrasensitive Electrochemical Detection of MiRNA Based on DNA Strand Displacement Polymerization and Ca^{2+} -Dependent DNAzyme Cleavage. *Analyst* **2018**, *143* (22), 5352–5357. https://doi.org/10.1039/C8AN01555D.

(41) Roy, N.; Magee, M.; Kiessling, B. The Use of the ISTAT Portable Analyzer in Patients Undergoing Cardiopulmonary Bypass. *J. Clin. Monit.* **1996**, *12* (4), 311–315. https://doi.org/10.1007/bf02221752.

(42) Pereira da Silva Neves, M. M.; González-García, M. B.; Hernández-Santos, D.; Fanjul-Bolado, P. Future Trends in the Market for Electrochemical Biosensing. *Current Opinion in Electrochemistry*. Elsevier B.V. August 2018, pp 107–111. https://doi.org/10.1016/j.coelec.2018.05.002.

(43) Pandey, R.; Chang, D.; Smieja, M.; Hoare, T.; Li, Y.; Soleymani, L. Integrating Programmable DNAzymes with Electrical Readout for Rapid and Culture-Free Bacterial Detection Using a Handheld Platform. *Nat. Chem.* **2021**. https://doi.org/10.1038/s41557-021-00718-x.

(44) Hassani, S.; Akmal, M. R.; Salek-Maghsoudi, A.; Rahmani, S.; Ganjali, M. R.; Norouzi, P.; Abdollahi, M. Novel Label-Free Electrochemical Aptasensor for Determination of Diazinon Using Gold Nanoparticles-Modified Screen-Printed Gold Electrode. *Biosens. Bioelectron.* **2018**. https://doi.org/10.1016/j.bios.2018.08.041.

(45) Radi, A.-E. Electrochemical Aptamer-Based Biosensors: Recent Advances and Perspectives. *Int. J. Electrochem.* **2011**, *2011*, 1–17. https://doi.org/10.4061/2011/863196.

(46) Li, H.; Li, S.; Xia, F. Electrochemical Sandwich Assays for Protein Detection. In

Biosensors Based on Sandwich Assays; Springer Singapore: Singapore, 2018; pp 47–68. https://doi.org/10.1007/978-981-10-7835-4_4.

(47) Singh, S.; Gill, A. A. S.; Nlooto, M.; Karpoormath, R. Prostate Cancer Biomarkers Detection Using Nanoparticles Based Electrochemical Biosensors. *Biosens. Bioelectron.* **2019**, *137*, 213–221. https://doi.org/10.1016/J.BIOS.2019.03.065.

(48) Chang, F. Y.; Chen, M. K.; Jang, L. S.; Wang, M. H. The Effect of 3D Interdigitated Microelectrodes on Electrochemical Impedance Spectroscopy. In *Proceedings - 2014 International Conference on Information Science, Electronics and Electrical Engineering, ISEEE 2014*; Institute of Electrical and Electronics Engineers Inc., 2014; Vol. 2, pp 855–859. https://doi.org/10.1109/InfoSEEE.2014.6947788.

(49) Trotter, M.; Borst, N.; Thewes, R.; von Stetten, F. Review: Electrochemical DNA Sensing – Principles, Commercial Systems, and Applications. *Biosens. Bioelectron.* **2020**, *154* (January), 112069. https://doi.org/10.1016/j.bios.2020.112069.

(50) Pellitero, M. A.; Shaver, A.; Arroyo-Currás, N. Critical Review—Approaches for the Electrochemical Interrogation of DNA-Based Sensors: A Critical Review. *J. Electrochem. Soc.* **2020**, *167* (3), 037529. https://doi.org/10.1149/2.0292003JES.

(51) Ferapontova, E. E. Electron Transfer in DNA at Electrified Interfaces. *Chem. – An Asian J.* **2019**, *14* (21), 3773–3781. https://doi.org/10.1002/asia.201901024.

(52) Altman, S. The Road to RNase P. *Nat. Struct. Biol.* **2000**, *7* (10), 827–828. https://doi.org/10.1038/79566.

(53) Tuerk, C.; Gold, L. Systematic Evolution of Ligands by Exponential Enrichment: RNA Ligands to Bacteriophage T4 DNA Polymerase. *Science* **1990**, *249* (4968), 505–510. https://doi.org/10.1126/science.2200121.

(54) Ellington, A. D.; Szostak, J. W. In Vitro Selection of RNA Molecules That Bind Specific Ligands. *Nature* **1990**, *346* (6287), 818–822. https://doi.org/10.1038/346818a0.

(55) Ellington, A.; Szostak, J. Selection in Vitro of Single-Stranded DNA Molecules That Fold into Specific Ligand-Binding Structures. *Nature* **1992**, *355*, 850–852. https://doi.org/10.1038/355850a0.

(56) Robertson, D. L.; Joyce, G. F. Selection in Vitro of an RNA Enzyme That Specifically Cleaves Single-Stranded DNA. *Nature* **1990**, *344* (6265), 467–468. https://doi.org/10.1038/344467a0.

(57) Breaker, R. R.; Joyce, G. F. A DNA Enzyme That Cleaves RNA. *Chem. Biol.* **1994**, *1* (4), 223–229. https://doi.org/10.1016/1074-5521(94)90014-0.

(58) McConnell, E. M.; Cozma, I.; Morrison, D.; Li, Y. Biosensors Made of Synthetic Functional Nucleic Acids Toward Better Human Health. *Anal. Chem.* **2020**, *92* (1), 327–344. https://doi.org/10.1021/acs.analchem.9b04868.

(59) Gong, L.; Zhao, Z.; Lv, Y.-F.; Huan, S.-Y.; Fu, T.; Zhang, X.-B.; Shen, G.-L.; Yu, R.-Q. DNAzyme-Based Biosensors and Nanodevices. *Chem. Commun.* **2015**, *51* (6), 979–995. https://doi.org/10.1039/C4CC06855F.

(60) McConnell, E. M.; Morrison, D.; Rey Rincon, M. A.; Salena, B. J.; Li, Y. Selection and Applications of Synthetic Functional DNAs for Bacterial Detection. *TrAC Trends Anal. Chem.* **2020**, *124*, 115785. https://doi.org/10.1016/j.trac.2019.115785.

(61) Zhou, W.; Ding, J.; Liu, J. Theranostic DNAzymes. *Theranostics* **2017**, *7* (4), 1010–1025. https://doi.org/10.7150/thno.17736.

(62) Zhou, W.; Saran, R.; Liu, J. Metal Sensing by DNA. *Chem. Rev.* **2017**, *117* (12), 8272–8325. https://doi.org/10.1021/acs.chemrev.7b00063.

(63) Sinha, A.; Gopinathan, P.; Chung, Y. Da; Lin, H. Y.; Li, K. H.; Ma, H. P.; Huang, P. C.; Shiesh, S. C.; Lee, G. Bin. An Integrated Microfluidic Platform to Perform Uninterrupted SELEX Cycles to Screen Affinity Reagents Specific to Cardiovascular Biomarkers. *Biosens. Bioelectron.* **2018**, *122* (September), 104–112. https://doi.org/10.1016/j.bios.2018.09.040.

(64) Hünniger, T.; Wessels, H.; Fischer, C.; Paschke-Kratzin, A.; Fischer, M. Just in Time-Selection: A Rapid Semiautomated SELEX of DNA Aptamers Using Magnetic Separation and BEAMing. *Anal. Chem.* **2014**, *86* (21), 10940–10947. https://doi.org/10.1021/ac503261b.

(65) Kumar, S.; Jain, S.; Dilbaghi, N.; Ahluwalia, A. S.; Hassan, A. A.; Kim, K.-H. Advanced Selection Methodologies for DNAzymes in Sensing and Healthcare Applications. *Trends Biochem. Sci.* **2019**, *44* (3), 190–213. https://doi.org/10.1016/j.tibs.2018.11.001.

(66) Hickling, A. Studies in Electrode Polarisation. Part IV.—The Automatic Control of the Potential of a Working Electrode. *Trans. Faraday Soc* **1942**, *38* (0), 27–33. https://doi.org/10.1039/tf9423800027.

(67) Palmsens. History of the potentiostat https://www.palmsens.com/knowledgebase-article/history-of-the-potentiostat/ (accessed Aug 26, 2021).

(68) Dryden, M. D. M.; Wheeler, A. R. DStat: A Versatile, Open-Source Potentiostat for Electroanalysis and Integration. *PLoS One* **2015**, *10* (10). https://doi.org/10.1371/journal.pone.0140349.

(69) Zahner. Scientific Instrumentation- Zahner IM6 Spezifications. *216* (4547), 687.

(70) Ainla, A.; Mousavi, M. P. S.; Tsaloglou, M. N.; Redston, J.; Bell, J. G.; Fernández-Abedul, M. T.; Whitesides, G. M. Open-Source Potentiostat for Wireless Electrochemical Detection with Smartphones. *Anal. Chem.* **2018**, *90* (10), 6240–6246. https://doi.org/10.1021/acs.analchem.8b00850.

(71) Dryden, M. D. M.; Wheeler, A. R. DStat: A Versatile, Open-Source Potentiostat for Electroanalysis and Integration. *PLoS One* **2015**, *10* (10), 1–17. https://doi.org/10.1371/journal.pone.0140349.

(72) Rowe, A. A.; Bonham, A. J.; White, R. J.; Zimmer, M. P.; Yadgar, R. J.; Hobza, T. M.; Honea, J. W.; Ben-Yaacov, I.; Plaxco, K. W. Cheapstat: An Open-Source, "Do-It-Yourself" Potentiostat for Analytical and Educational Applications. *PLoS One* **2011**, *6* (9). https://doi.org/10.1371/journal.pone.0023783.

(73) Cordova-Huaman, A. V.; Jauja-Ccana, V. R.; La Rosa-Toro, A. Low-Cost Smartphone-Controlled Potentiostat Based on Arduino for Teaching Electrochemistry Fundamentals and Applications. *Heliyon* **2021**, *7* (2), e06259. https://doi.org/10.1016/j.heliyon.2021.e06259.

(74) Li, Y. C.; Melenbrink, E. L.; Cordonier, G. J.; Boggs, C.; Khan, A.; Isaac, M. K.; Nkhonjera, L. K.; Bahati, D.; Billinge, S. J.; Haile, S. M.; Kreuter, R. A.; Crable, R. M.; Mallouk, T. E. An Easily Fabricated Low-Cost Potentiostat Coupled with User-Friendly Software for Introducing Students to Electrochemical Reactions and Electroanalytical Techniques. *J. Chem. Educ.* **2018**, *95* (9), 1658–1661. https://doi.org/10.1021/acs.jchemed.8b00340.

(75) Meloni, G. N. Building a Microcontroller Based Potentiostat: A Inexpensive and Versatile Platform for Teaching Electrochemistry and Instrumentation. *J. Chem. Educ.* **2016**, *93* (7), 1320–1322. https://doi.org/10.1021/acs.jchemed.5b00961.

(76) Irving, P.; Cecil, R.; Yates, M. Z. MYSTAT: A Compact Potentiostat/Galvanostat for

General Electrochemistry Measurements. *HardwareX* **2021**, *9*, e00163. https://doi.org/10.1016/j.ohx.2020.e00163.

(77) Hoilett, O. S.; Walker, J. F.; Balash, B. M.; Jaras, N. J.; Boppana, S.; Linnes, J. C. Kickstat: A Coin-Sized Potentiostat for High-Resolution Electrochemical Analysis. *Sensors (Switzerland)* **2020**, *20* (8), 1–12. https://doi.org/10.3390/s20082407.

(78) Adams, S. D.; Doeven, E. H.; Quayle, K.; Kouzani, A. Z. MiniStat: Development and Evaluation of a Mini-Potentiostat for Electrochemical Measurements. *IEEE Access* **2019**. https://doi.org/10.1109/ACCESS.2019.2902575.

(79) Glasscott, M. W.; Verber, M. D.; Hall, J. R.; Pendergast, A. D.; McKinney, C. J.; Dick, J. E. SweepStat: A Build-It-Yourself, Two-Electrode Potentiostat for Macroelectrode and Ultramicroelectrode Studies. *J. Chem. Educ.* **2020**, *97* (1), 265–270. https://doi.org/10.1021/acs.jchemed.9b00893.

(80) Jenkins, D. M.; Lee, B. E.; Jun, S.; Reyes-De-Corcuera, J.; McLamore, E. S. ABE-Stat, a Fully Open-Source and Versatile Wireless Potentiostat Project Including Electrochemical Impedance Spectroscopy. *J. Electrochem. Soc.* **2019**, *166* (9), B3056–B3065. https://doi.org/10.1149/2.0061909jes.

(81) Krorakai, K.; Klangphukhiew, S.; Kulchat, S.; Patramanon, R. Smartphone-Based Nfc Potentiostat for Wireless Electrochemical Sensing. *Appl. Sci.* **2021**, *11* (1), 1–13. https://doi.org/10.3390/app11010392.

(82) Barragan, J. T. C.; Kubota, L. T. Minipotentiostat Controlled by Smartphone on a Micropipette: A Versatile, Portable, Agile and Accurate Tool for Electroanalysis. *Electrochim. Acta* **2020**, *341*. https://doi.org/10.1016/j.electacta.2020.136048.

(83) Guo, J. Smartphone-Powered Electrochemical Dongle for Point-of-Care Monitoring of Blood β-Ketone. *Anal. Chem.* **2017**, *89* (17), 8609–8613. https://doi.org/10.1021/acs.analchem.7b02531.

(84) Yoo, E. H.; Lee, S. Y. Glucose Biosensors: An Overview of Use in Clinical Practice. *Sensors* **2010**, *10* (5), 4558–4576. https://doi.org/10.3390/s100504558.

(85) Xie, H.; Di, K.; Huang, R.; Khan, A.; Xia, Y.; Xu, H.; Liu, C.; Tan, T.; Tian, X.; Shen, H.; He, N.; Li, Z. Extracellular Vesicles Based Electrochemical Biosensors for Detection of Cancer Cells: A Review. *Chinese Chem. Lett.* **2020**, *31* (7), 1737–1745. https://doi.org/10.1016/j.cclet.2020.02.049.

(86) Diculescu, V. C.; Chiorcea-Paquim, A. M.; Oliveira-Brett, A. M. Applications of a DNA-Electrochemical Biosensor. *TrAC - Trends in Analytical Chemistry*. Elsevier B.V. May 1, 2016, pp 23–36. https://doi.org/10.1016/j.trac.2016.01.019.

(87) Pfeiffer, F.; Mayer, G. Selection and Biosensor Application of Aptamers for Small Molecules. *Front. Chem.* **2016**, *4* (JUN), 1–21. https://doi.org/10.3389/fchem.2016.00025.

(88) Hammond, J. L.; Formisano, N.; Estrela, P.; Carrara, S.; Tkac, J. Electrochemical Biosensors and Nanobiosensors. *Essays Biochem.* **2016**, *60* (1), 69–80. https://doi.org/10.1042/EBC20150008.

(89) Turner, A. P. F. Biosensors: Sense and Sensibility. *Chem. Soc. Rev.* **2013**, *42* (8), 3184–3196. https://doi.org/10.1039/c3cs35528d.

(90) Bianchi, V.; Boni, A.; Fortunati, S.; Giannetto, M.; Careri, M.; De Munari, I. A Wi-Fi Cloud-Based Portable Potentiostat for Electrochemical Biosensors. *IEEE Trans. Instrum. Meas.* **2020**, *69* (6), 3232–3240. https://doi.org/10.1109/TIM.2019.2928533.

(91) Fan, Y.; Liu, J.; Wang, Y.; Luo, J.; Xu, H.; Xu, S.; Cai, X. A Wireless Point-of-Care Testing System for the Detection of Neuron-Specific Enolase with Microfluidic Paper-

Based Analytical Devices. *Biosens. Bioelectron.* **2017**, *95* (April), 60–66. https://doi.org/10.1016/j.bios.2017.04.003.
(92) Jafari, H. M.; Genov, R. Chopper-Stabilized Bidirectional Current Acquisition Circuits for Electrochemical Amperometric Biosensors. *IEEE Trans. Circuits Syst. I Regul. Pap.* **2013**, *60* (5), 1149–1157. https://doi.org/10.1109/TCSI.2013.2248771.
(93) Shen, X.; Ju, F.; Li, G.; Ma, L. Smartphone-Based Electrochemical Potentiostat Detection System Using Pedot: Pss/Chitosan/Graphene Modified Screen-Printed Electrodes for Dopamine Detection. *Sensors (Switzerland)* **2020**, *20* (10). https://doi.org/10.3390/s20102781.
(94) Sepúlveda, F.; Hernández, J.; Manríquez, A. Construction of a Potentiostat to Perform Electrochemical Impedance Spectroscopy (EIS) Tests. *Mod. Instrum.* **2017**, *06* (02), 15–27. https://doi.org/10.4236/mi.2017.62002.
(95) Ji, D.; Liu, L.; Li, S.; Chen, C.; Lu, Y.; Wu, J.; Liu, Q. Smartphone-Based Cyclic Voltammetry System with Graphene Modified Screen Printed Electrodes for Glucose Detection. *Biosens. Bioelectron.* **2017**, *98* (March), 449–456. https://doi.org/10.1016/j.bios.2017.07.027.
(96) Ramfos, I.; Vassiliadis, N.; Blionas, S.; Efstathiou, K.; Fragoso, A.; O'Sullivan, C. K.; Birbas, A. A Compact Hybrid-Multiplexed Potentiostat for Real-Time Electrochemical Biosensing Applications. *Biosens. Bioelectron.* **2013**, *47*, 482–489. https://doi.org/10.1016/j.bios.2013.03.068.
(97) Giordano, G. F.; Vicentini, M. B. R.; Murer, R. C.; Augusto, F.; Ferrão, M. F.; Helfer, G. A.; da Costa, A. B.; Gobbi, A. L.; Hantao, L. W.; Lima, R. S. Point-of-Use Electroanalytical Platform Based on Homemade Potentiostat and Smartphone for Multivariate Data Processing. *Electrochim. Acta* **2016**, *219*, 170–177. https://doi.org/10.1016/j.electacta.2016.09.157.
(98) Dobbelaere, T.; Vereecken, P. M.; Detavernier, C. A USB-Controlled Potentiostat/Galvanostat for Thin-Film Battery Characterization. *HardwareX* **2017**, *2*, 34–49. https://doi.org/10.1016/j.ohx.2017.08.001.
(99) Ainla, A.; Mousavi, M. P. S.; Tsaloglou, M. N.; Redston, J.; Bell, J. G.; Fernández-Abedul, M. T.; Whitesides, G. M. Open-Source Potentiostat for Wireless Electrochemical Detection with Smartphones. *Anal. Chem.* **2018**, *90* (10), 6240–6246. https://doi.org/10.1021/acs.analchem.8b00850.
(100) Siegert, M. A Scalable Multi-Channel Software Potentiostat. *Front. Energy Res.* **2018**, *6* (November), 1–4. https://doi.org/10.3389/fenrg.2018.00131.
(101) Paleček, E.; Fojta, M. Magnetic Beads as Versatile Tools for Electrochemical DNA and Protein Biosensing. *Talanta* **2007**, *74* (3), 276–290. https://doi.org/10.1016/j.talanta.2007.08.020.
(102) van Welie, M. BLESSED BLE. 2021.
(103) Jahoda, P. MPAndroidChart. 2021.
(104) Rzeźnicki, M. SGFilter. 2021.
(105) Ali, M. M.; Brown, C. L.; Jahanshahi-Anbuhi, S.; Kannan, B.; Li, Y.; Filipe, C. D. M.; Brennan, J. D. A Printed Multicomponent Paper Sensor for Bacterial Detection. *Sci. Rep.* **2017**, *7* (1), 1–10. https://doi.org/10.1038/s41598-017-12549-3.
(106) Colburn, A. W.; Levey, K. J.; O'Hare, D.; Macpherson, J. V. Lifting the Lid on the Potentiostat: A Beginner's Guide to Understanding Electrochemical Circuitry and Practical Operation. *Phys. Chem. Chem. Phys.* **2021**, *23* (14), 8100–8117.

https://doi.org/10.1039/d1cp00661d.
(107) Ju, H. Signal Amplification for Highly Sensitive Bioanalysis Based on Biosensors or Biochips. *J. Biochips Tissue Chips* **2012**, *02* (02), 2–3. https://doi.org/10.4172/2153-0777.1000e114.
(108) Acharya, D.; Rani, A.; Agarwal, S.; Singh, V. Application of Adaptive Savitzky–Golay Filter for EEG Signal Processing. *Perspect. Sci.* **2016**, *8*, 677–679. https://doi.org/10.1016/j.pisc.2016.06.056.
(109) Feuerstein, D.; Parker, K. H.; Boutelle, M. G. Practical Methods for Noise Removal: Applications to Spikes, Nonstationary Quasi-Periodic Noise, and Baseline Drift. *Anal. Chem.* **2009**, *81* (12), 4987–4994. https://doi.org/10.1021/ac900161x.
(110) Gonçalves, W. D.; Lanfredi, A. J. C.; Crespilho, F. N. Development of Numerical Methods for Signal Smoothing and Noise Modeling in Single Wire-Based Electrochemical Biosensors. *J. Phys. Chem. C* **2011**, *115* (32), 16172–16179. https://doi.org/10.1021/jp204180e.
(111) Górski, Ł.; Ciepiela, F.; Jakubowska, M. Automatic Baseline Correction in Voltammetry. *Electrochim. Acta* **2014**, *136*, 195–203. https://doi.org/10.1016/j.electacta.2014.05.076.
(112) Bard, A. J.; Faulkner, L. R. *Electrochemical Methods: Fundamentals and Applications*, 2nd ed.; Wiley-Interscience: New York, New York, United States, 2000.
(113) Ren, K.; Wu, J.; Yan, F.; Ju, H. Ratiometric Electrochemical Proximity Assay for Sensitive One-Step Protein Detection. *Sci. Rep.* **2014**, *4*, 1–6. https://doi.org/10.1038/srep04360.
(114) Aidoo-Brown, J.; Moschou, D.; Estrela, P. Multiplexed Prostate Cancer Companion Diagnostic Devices. *Sensors* **2021**, *21* (15). https://doi.org/10.3390/s21155023.
(115) Tang, Z.; Ma, Z. Ratiometric Ultrasensitive Electrochemical Immunosensor Based on Redox Substrate and Immunoprobe. *Sci. Rep.* **2016**, *6* (September), 2–7. https://doi.org/10.1038/srep35440.
(116) Yáñez-Sedeño, P.; Campuzano, S.; Pingarrón, J. M. Multiplexed Electrochemical Immunosensors for Clinical Biomarkers. *Sensors (Switzerland)* **2017**, *17* (5). https://doi.org/10.3390/s17050965.
(117) Liu, M.; Zhang, Q.; Brennan, J. D.; Li, Y. Graphene-DNAzyme-Based Fluorescent Biosensor for Escherichia Coli Detection. *MRS Commun.* **2018**, *8* (3), 687–694. https://doi.org/10.1557/mrc.2018.97.
(118) Zhang, J. RNA-Cleaving DNAzymes: Old Catalysts with New Tricks for Intracellular and in Vivo Applications. *Catalysts* **2018**, *8* (11), 1–20. https://doi.org/10.3390/catal8110550.
(119) Soleymani, L.; Li, F. Mechanistic Challenges and Advantages of Biosensor Miniaturization into the Nanoscale. *ACS Sensors*. American Chemical Society April 2017, pp 458–467. https://doi.org/10.1021/acssensors.7b00069.
(120) Mohanty, S. P.; Koucianos, E. Biosensors: A Tutorial Review. *IEEE Potentials* **2006**, *25* (2), 35–40. https://doi.org/10.1109/MP.2006.1649009.
(121) Mehrotra, P. Biosensors and Their Applications - A Review. *J. Oral Biol. Craniofacial Res.* **2016**, *6* (2), 153–159. https://doi.org/10.1016/j.jobcr.2015.12.002.
(122) Victorious, A.; Saha, S.; Pandey, R.; Didar, T. F.; Soleymani, L. Affinity-Based Detection of Biomolecules Using Photo-Electrochemical Readout. *Frontiers in Chemistry*. Frontiers Media S.A. September 2019. https://doi.org/10.3389/fchem.2019.00617.
(123) Hosseini, A.; Pandey, R.; Osman, E.; Victorious, A.; Li, F.; Didar, T.; Soleymani, L. Roadmap to the Bioanalytical Testing of COVID-19: From Sample Collection to Disease

Surveillance. *ACS Sensors* **2020**, *5* (11), 3328–3345. https://doi.org/10.1021/acssensors.0c01377.
(124) Beltrán Lopez, A. P. DNA Biosensors and Biomarkers to Cancer Detection. *Int. J. Biosens. Bioelectron.* **2018**, *4* (1), 20–21. https://doi.org/10.15406/ijbsbe.2018.04.00090.
(125) Khan, M. A.; Mujahid, M. Recent Advances in Electrochemical and Optical Biosensors Designed for Detection of Interleukin 6. *Sensors (Switzerland)* **2020**, *20* (3), 1–27. https://doi.org/10.3390/s20030646.
(126) Metkar, S. K.; Girigoswami, K. Diagnostic Biosensors in Medicine – A Review. *Biocatal. Agric. Biotechnol.* **2019**, *17* (December 2018), 271–283. https://doi.org/10.1016/j.bcab.2018.11.029.
(127) King, K. R.; Grazette, L. P.; Paltoo, D. N.; McDevitt, J. T.; Sia, S. K.; Barrett, P. M.; Apple, F. S.; Gurbel, P. A.; Weissleder, R.; Leeds, H.; Iturriaga, E. J.; Rao, A. K.; Adhikari, B.; Desvigne-Nickens, P.; Galis, Z. S.; Libby, P. Point-of-Care Technologies for Precision Cardiovascular Care and Clinical Research: National Heart, Lung, and Blood Institute Working Group. *JACC Basic to Transl. Sci.* **2016**, *1* (1–2), 73–86. https://doi.org/10.1016/j.jacbts.2016.01.008.
(128) Harpaz, D.; Eltzov, E.; Seet, R. C. S.; Marks, R. S.; Tok, A. I. Y. Point-of-Care-Testing in Acute Stroke Management: An Unmet Need Ripe for Technological Harvest. *Biosensors* **2017**, *7* (3), 30. https://doi.org/10.3390/bios7030030.
(129) Quinchia, J.; Echeverri, D.; Cruz-Pacheco, A. F.; Maldonado, M. E.; Orozco, J. A. Electrochemical Biosensors for Determination of Colorectal Tumor Biomarkers. *Micromachines* **2020**, *11* (4), 1–46. https://doi.org/10.3390/MI11040411.
(130) Saha, S.; Victorious, A.; Pandey, R.; Clifford, A.; Zhitomirsky, I.; Soleymani, L. Differential Photoelectrochemical Biosensing Using DNA Nanospacers to Modulate Electron Transfer between Metal and Semiconductor Nanoparticles. *ACS Appl. Mater. Interfaces* **2020**, *12* (33), 36895–36905. https://doi.org/10.1021/acsami.0c09443.
(131) Sakib, S.; Bakhshandeh, F.; Saha, S.; Soleymani, L.; Zhitomirsky, I. Surface Functionalization of Metal Oxide Semiconductors with Catechol Ligands for Enhancing Their Photoactivity. *Sol. RRL n/a* (n/a), 2100512. https://doi.org/https://doi.org/10.1002/solr.202100512.
(132) Sakib, S.; Pandey, R.; Soleymani, L.; Zhitomirsky, I. Surface Modification of TiO_2 for Photoelectrochemical DNA Biosensors. *Med. DEVICES SENSORS* **2020**, *3* (2). https://doi.org/10.1002/mds3.10066.
(133) Roy, S.; Gao, Z. Nanostructure-Based Electrical Biosensors. *Nano Today* **2009**, *4* (4), 318–334. https://doi.org/10.1016/j.nantod.2009.06.003.
(134) Chalklen, T.; Jing, Q.; Kar-Narayan, S. Biosensors Based on Mechanical and Electrical Detection Techniques. *Sensors (Switzerland)* **2020**, *20* (19), 26–37. https://doi.org/10.3390/s20195605.
(135) Chen, J. X.; Zhuo, Y.; Peng, X.; Chai, Y. Q.; Yuan, R.; Liang, W. Bin. A Dynamic DNA Machine via Free Walker Movement on Lipid Bilayer for Ultrasensitive Electrochemiluminescent Bioassay. *Anal. Chem.* **2019**, *91* (21), 14125–14132. https://doi.org/10.1021/acs.analchem.9b03999.
(136) Escobedo, P.; Erenas, M. M.; Martínez-Olmos, A.; Carvajal, M. A.; Gonzalez-Chocano, S.; Capitán-Vallvey, L. F.; Palma, A. J. General-Purpose Passive Wireless Point–of–Care Platform Based on Smartphone. *Biosens. Bioelectron.* **2019**, *141*, 1–23. https://doi.org/10.1016/j.bios.2019.111360.

(137) Arlett, J. L.; Myers, E. B.; Roukes, M. L. Comparative Advantages of Mechanical Biosensors. *Nat. Nanotechnol.* **2011**, *6* (4), 203–215. https://doi.org/10.1038/nnano.2011.44.
(138) Vigneshvar, S.; Sudhakumari, C. C.; Senthilkumaran, B.; Prakash, H. Recent Advances in Biosensor Technology for Potential Applications - an Overview. *Front. Bioeng. Biotechnol.* **2016**, *4* (FEB), 1–9. https://doi.org/10.3389/fbioe.2016.00011.
(139) Golub, E.; Pelossof, G.; Freeman, R.; Zhang, H.; Willner, I. Electrochemical, Photoelectrochemical, and Surface Plasmon Resonance Detection of Cocaine Using Supramolecular Aptamer Complexes and Metallic or Semiconductor Nanoparticles. *Anal. Chem.* **2009**, *81* (22), 9291–9298. https://doi.org/10.1021/ac901551q.
(140) Saha, S.; Chan, Y.; Soleymani, L. Enhancing the Photoelectrochemical Response of DNA Biosensors Using Wrinkled Interfaces. *ACS Appl. Mater. Interfaces* **2018**, *10* (37), 31178–31185. https://doi.org/10.1021/acsami.8b12286.
(141) Sakib, S.; Hosseini, A.; Zhitomirsky, I.; Soleymani, L. Photoelectrochemical IL-6 Immunoassay Manufactured on Multifunctional Catecholate-Modified TiO 2 Scaffolds . *ACS Appl. Mater. Interfaces* **2021**. https://doi.org/10.1021/acsami.1c18240.
(142) Yagura, T.; Makita, K.; Yamamoto, H.; Menck, C. F. M.; Schuch, A. P. Biological Sensors for Solar Ultraviolet Radiation. *Sensors (Switzerland)* **2011**, *11* (4), 4277–4294. https://doi.org/10.3390/s110404277.
(143) Han, Z.; Luo, M.; Chen, L.; Pan, H.; Chen, J.; Li, C. A Photoelectrochemical Biosensor for Determination of DNA Based on Flower Rod-like Zinc Oxide Heterostructures. *Microchim. Acta* **2017**, *184* (8), 2541–2549. https://doi.org/10.1007/s00604-017-2257-5.
(144) Zhang, X.; Zhao, Y.; Li, S.; Zhang, S. Photoelectrochemical Biosensor for Detection of Adenosine Triphosphate in the Extracts of Cancer Cells. *Chem. Commun.* **2010**, *46* (48), 9173–9175. https://doi.org/10.1039/c0cc03595e.
(145) Wang, W.; Bao, L.; Lei, J.; Tu, W.; Ju, H. Visible Light Induced Photoelectrochemical Biosensing Based on Oxygen-Sensitive Quantum Dots. *Anal. Chim. Acta* **2012**, *744*, 33–38. https://doi.org/10.1016/j.aca.2012.07.025.
(146) Zhang, X.; Xu, F.; Zhao, B.; Ji, X.; Yao, Y.; Wu, D.; Gao, Z.; Jiang, K. Synthesis of CdS Quantum Dots Decorated Graphene Nanosheets and Non-Enzymatic Photoelectrochemical Detection of Glucose. *Electrochim. Acta* **2014**, *133*, 615–622. https://doi.org/10.1016/j.electacta.2014.04.089.
(147) Yue, Z.; Lisdat, F.; Parak, W. J.; Hickey, S. G.; Tu, L.; Sabir, N.; Dorfs, D.; Bigall, N. C. Quantum-Dot-Based Photoelectrochemical Sensors for Chemical and Biological Detection. *ACS Appl. Mater. Interfaces* **2013**, *5* (8), 2800–2814. https://doi.org/10.1021/am3028662.
(148) Zhang, X.; Xu, Y.; Yang, Y.; Jin, X.; Ye, S.; Zhang, S.; Jiang, L. A New Signal-on Photoelectrochemical Biosensor Based on a Graphene/Quantum-Dot Nanocomposite Amplified by the Dual-Quenched Effect of Bipyridinium Relay and AuNPs. *Chem. - A Eur. J.* **2012**, *18* (51), 16411–16418. https://doi.org/10.1002/chem.201202213.
(149) Li, Z.; Zhang, J.; Li, Y.; Zhao, S.; Zhang, P.; Zhang, Y.; Bi, J.; Liu, G.; Yue, Z. Carbon Dots Based Photoelectrochemical Sensors for Ultrasensitive Detection of Glutathione and Its Applications in Probing of Myocardial Infarction. *Biosens. Bioelectron.* **2018**, *99*, 251–258. https://doi.org/10.1016/j.bios.2017.07.065.
(150) Gergeroglu, H.; Yildirim, S.; Ebeoglugil, M. F. Nano-Carbons in Biosensor Applications: An Overview of Carbon Nanotubes (CNTs) and Fullerenes (C60). *SN Appl. Sci.* **2020**, *2*

(4). https://doi.org/10.1007/s42452-020-2404-1.
(151) Saha, S.; Victorious, A.; Pandey, R.; Clifford, A.; Zhitomirsky, I.; Soleymani, L. Differential Photoelectrochemical Biosensing Using DNA Nanospacers to Modulate Electron Transfer between Metal and Semiconductor Nanoparticles. *ACS Appl. Mater. Interfaces* **2020**, *12* (33), 36895–36905. https://doi.org/10.1021/acsami.0c09443.
(152) Špačková, B.; Wrobel, P.; Bocková, M.; Homola, J. Optical Biosensors Based on Plasmonic Nanostructures: A Review. *Proc. IEEE* **2016**, *104* (12), 2380–2408. https://doi.org/10.1109/JPROC.2016.2624340.
(153) Kongkanand, A.; Domınguez, R. M.; Kamat, P. V. Single Wall Carbon Nanotube Scaffolds for Photoelectrochemical Solar Cells. Capture and Transport of Photogenerated Electrons. *Nano Lett.* **2007**, *7* (3), 676–680. https://doi.org/10.3141/1528-08.
(154) Han, C.; Li, Y. H.; Qi, M. Y.; Zhang, F.; Tang, Z. R.; Xu, Y. J. Surface/Interface Engineering of Carbon-Based Materials for Constructing Multidimensional Functional Hybrids. *Sol. RRL* **2020**, *4* (8), 1–25. https://doi.org/10.1002/solr.201900577.
(155) Arbouch, I.; Cornil, D.; Karzazi, Y.; Hammouti, B.; Lazzaroni, R.; Cornil, J. Influence of the Nature of the Anchoring Group on Electron Injection Processes at Dye-Titania Interfaces. *Phys. Chem. Chem. Phys.* **2017**, *19* (43), 29389–29401. https://doi.org/10.1039/c7cp05638a.
(156) Fan, G. C.; Ren, X. L.; Zhu, C.; Zhang, J. R.; Zhu, J. J. A New Signal Amplification Strategy of Photoelectrochemical Immunoassay for Highly Sensitive Interleukin-6 Detection Based on TiO2/CdS/CdSe Dual Co-Sensitized Structure. *Biosens. Bioelectron.* **2014**, *59*, 45–53. https://doi.org/10.1016/j.bios.2014.03.011.
(157) Sarkar, S.; Makhal, A.; Lakshman, K.; Bora, T.; Dutta, J.; Kumar Pal, S. Dual-Sensitization via Electron and Energy Harvesting in CdTe Quantum Dots Decorated ZnO Nanorod-Based Dye-Sensitized Solar Cells. *J. Phys. Chem. C* **2012**, *116* (27), 14248–14256. https://doi.org/10.1021/jp3046593.
(158) Sun, A.; Wambach, T.; Venkatesh, A. G.; Hall, D. A. A Low-Cost Smartphone-Based Electrochemical Biosensor for Point-of-Care Diagnostics. In *IEEE 2014 Biomedical Circuits and Systems Conference, BioCAS 2014 - Proceedings*; 2014. https://doi.org/10.1109/BioCAS.2014.6981725.
(159) Tsujiko, A.; Itoh, H.; Kisumi, T.; Shiga, A.; Murakoshi, K.; Nakato, Y. Observation of Cathodic Photocurrents at Nanocrystalline TiO2 Film Electrodes, Caused by Enhanced Oxygen Reduction in Alkaline Solutions. *J. Phys. Chem. B* **2002**, *106* (23), 5878–5885. https://doi.org/10.1021/jp012144l.
(160) Dumortier, M.; Bosserez, T.; Rongé, J.; Martens, J. A.; Haussener, S. Combined Experimental-Numerical Analysis of Transient Phenomena in a Photoelectrochemical Water Splitting Cell. *J. Phys. Chem. C* **2016**, *120* (7), 3705–3714. https://doi.org/10.1021/acs.jpcc.5b12445.
(161) Changshi, L. Energy and Charge Conservation during Photo Capacitance-Voltage. *Energy* **2021**, *214*, 118899. https://doi.org/10.1016/j.energy.2020.118899.
(162) ZAHNER-elektrik GmbH & Co. KG. specifications_zennium_electrochemcial_workstations.pdf http://zahner.de/files/specifications_zennium_electrochemcial_workstations.pdf (accessed Aug 23, 2021).
(163) Fu, Y.; Sun, D.; Chen, Y.; Huang, R.; Ding, Z.; Fu, X.; Li, Z. An Amine-Functionalized Titanium Metal-Organic Framework Photocatalyst with Visible-Light-Induced Activity

for CO 2 Reduction. *Angew. Chemie - Int. Ed.* **2012**, *51* (14), 3364–3367. https://doi.org/10.1002/anie.201108357.

(164) Zhang, X.; Li, S.; Jin, X.; Li, X. Aptamer Based Photoelectrochemical Cytosensor with Layer-by-Layer Assembly of CdSe Semiconductor Nanoparticles as Photoelectrochemically Active Species. *Biosens. Bioelectron.* **2011**, *26* (8), 3674–3678. https://doi.org/10.1016/j.bios.2011.01.030.

(165) Li, Y.; Xu, Y.; Fleischer, C. C.; Huang, J.; Lin, R.; Yang, L.; Mao, H. Impact of Anti-Biofouling Surface Coatings on the Properties of Nanomaterials and Their Biomedical Applications. *Journal of Materials Chemistry B*. Royal Society of Chemistry 2017, pp 9–24. https://doi.org/10.1039/c7tb01695f.

(166) Brynda, E.; Houska, M.; Brandenburg, A.; Wikerstål, A. Optical Biosensors for Real-Time Measurement of Analytes in Blood Plasma. *Biosens. Bioelectron.* **2002**, *17* (8), 665–675. https://doi.org/10.1016/S0956-5663(02)00028-3.